UNIVERSITA' DEGLI STUDI DI NAPOLI FEDERICO II

DOTTORATO DI RICERCA IN BIOLOGIA APPLICATA
INDIRIZZO ECOLOGIA TERRESTRE, PIANTE E SUOLO
XXI CICLO

"Large scale CO_2 fluxes determination from terrestrial ecosystems by means of a mass balance approach "

Dottorando: dott.ssa Silvia Maria Alfieri

Tutore: Prof. Angelo Fierro
Tutori aggiunti: Prof. Angelo Riccio, Dott. Vincenzo Magliulo

Anni accademici 2006-2008

CO2 is the most important quantitatively greenhouse gas attributable to human activities. The precise geographical distribution of the sinks on the land and ocean surface is still a matter of considerable controversy and depends largely on the availability of data, which are necessary in model inversions.

It is important to understand the processes controlling the uptake of carbon dioxide by the surface, so that the exchange rate and variability can be predicted under the influence of climatic change.

From the perspective of the Kyoto protocol and UNFCC convention, Annex 1 countries are required to map source and sink distributions on a regional (national/state) scale, because anthropogenic emissions may be partially balanced by natural sinks. Therefore there is an increasing demand for methods to derive large scale carbon dioxide (CO_2) fluxes.

The flux of CO_2 is a direct measure of net ecosystem exchange and quantifies the transfer of carbon between atmospheric, terrestrial and oceanic stores. This is of particular interest given the current concern about rising CO_2 concentration in the atmosphere and the uncertainties in the sequestration of carbon in the terrestrial biosphere.

This thesis is focused to the implementation of a mass balance methodology to estimate CO_2 surface fluxes at territorial scale starting from aircraft measurements of wind and scalars in the lower layers of the atmosphere.

This work of thesis was born in prevision of the assessment of the method for the estimation of CH_4 and N_2O fluxes over the "Piana del Sele" landscape, an Italian coastal site located close to the city of Salerno. Mass balance method was identified as the only way to determine area average flux of such gas in that area. The first reason was the impossibilities to use Airborne Eddy covariance method for the determination of mass fluxes, missing appropriate instruments for measurements of such gas like methane (CH_4) and nitrogen oxide (N_2O) at the required frequency of 50 Hz (Cleugh et al, 2004, Gioli et al, 2007).

In Chapter 1 are explained the exchange processes dealing with the carbon cycle and most important effects due to the global enhancement of CO_2 concentration in the atmosphere. Chapter 2 introduces to the physic of the lowest layer of the atmosphere: the so called Atmospheric Boundary Layer. Most part of the processes of interaction

between the troposphere and the surface are confined within it. Important attention is given to the atmospheric phenomena linked to the spatial heterogeneity of the surface. In particular the “sea breeze effect”, occurring in the great part of the flight experiments presented in this thesis.

The on-board instrumentation of the Sky Arrow ERA aircraft is described in Chapter 3.

Among the methods reported in literature to estimate trace gases fluxes at territorial scale tree different one were selected : Airborne Eddy Covariance (Gioli et al, 2007) , “Low Level Flight with Inverse Modelling” (Bunge et al, 2006) and “Mass Balance” method (Wratt et al, 200; Kalthoff, 2002). The basic theory of the methods is described in Chapter 4. Mass balance approach requires such as regression procedures in order to integrate horizontal fluxes in the space. Two different methods are used in this thesis. The first one, based on a deterministic approach, was implemented in collaboration with the institute of the National Research Council, “Application of Calculation Mario Picone” (section 4.3.2.1). Bayesian Montecarlo Method, realized by Prof. Angelo Riccio of “Parthenope University” of Naples was also used (section 4.3.2.2).

A flight experiment was carried out over Piana del Sele Landscape in order to test the mass balance method. The experimental setup as well as results from the application are described in Chapter 5.

Industrial sites of Sardinia Island were also monitored with the main objective to obtain further applications of the method and to test the reliability of the results in different surfaces and meteorological conditions (Chapter 6).

Finally the tree method presented in Chapter 4 has been used to determine the averaged CO_2 flux, as well as to investigate about the spatial gradients of CO_2 flux in a territory close to the city of Forli (Chapter 7).

Chapter 1: Introduction

During the last centuries human activities have substantially modified biogeochemical cycles of the earth. The most important and the first to be understood has been the carbon cycle. The strong release of carbon that was stored in the prehistoric ecosystems (in fossil form) end in the vegetation has led to an increment in carbon dioxide (CO_2) concentrations from pre-industrial values of 280 ppm to 386 ppm in 2006. Sure this concentration have never been exceed in the last 420000 years, and probably in the last 200 million years.

Special efforts are doing in order to quantify future effect on climate change due to the increase of CO_2 concentrations and to understand the many components and interlinked process networks that comprise the terrestrial carbon cycle.

The Kyoto Protocol achieved a significant breakthrough by including terrestrial carbon sources and sinks into a legally binding emissions reduction framework. Moreover it scheduled the institution of a scientific commission, the Intergovernmental Panel on Climate Change, with the goal to assess the scientific, technical and socio-economic information relevant for the understanding of the risk of human-induced climate change

Global carbon cycle could be influenced by a lot of factors, among which the CO_2 atmospheric concentration itself. The increase in CO_2 concentrations has important effects on climate and could have fertilizing effects owing to acceleration of the uptake processes from ocean and land. Imbalances in the natural carbon cycle are also due to human activity, for example land conversion (from native vegetation to agriculture), and land management for carbon storage and fire suppression.

Better observational data and data access are necessary to improve understanding of ongoing changes, to better constrain model projections, and are a prerequisite for adaptive management required under conditions of climate change. Progress in knowledge depends on improved data availability.

1.1 The Carbon cycle

In Figure 1 are represented the main compartments of the carbon cycle and the estimation of the current storage in each compartments as well as the estimate the gross fluxes between them is shown. The additional flux (release to the atmosphere – positive; uptake – negative) associated with the human perturbation of the carbon cycle during the 1980s are showed in the left panel of Figure 1.

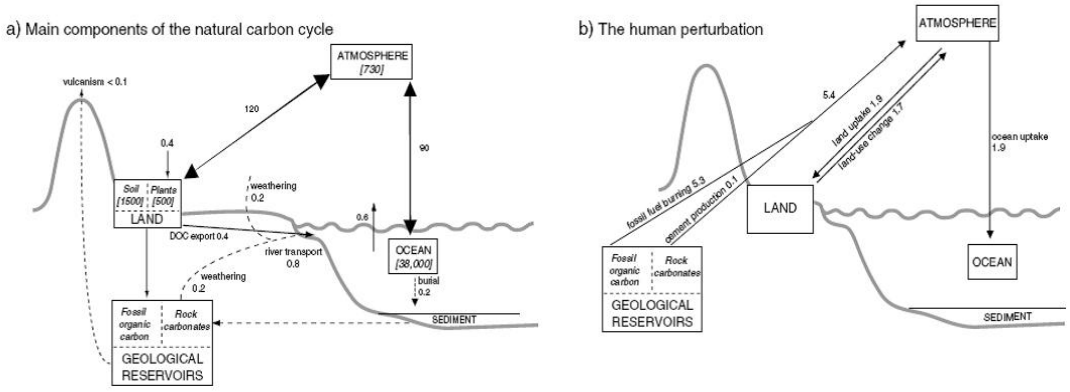

Figure 1: On the left panel: Scheme of the global carbon cycle and representation of carbon fluxes between the main ecosystems (biosphere, atmosphere and hydrosphere). In right panel are shown the human perturbations influencing the natural carbon cycle.

The major exchange processes are photosynthesis and respiration by plants (thick arrows in the left panel of Figure 1). The amount of these exchanges is 1000 times bigger than that due to geochemical exchange processes and works on smaller time scale, from years to centuries. Photosynthesis is the process by which plants used carbon in inorganic form and convert it in carbohydrates. The quantity of carbon used in this process is the Gross Primary Production (GPP). About a half of this quantity is incorporated into new biomass (plant tissues such as leaves, roots, wood etc...) and the rest goes back to the atmosphere by the autotrophic respiration process (Rh). The difference between GPP and Rh is the Net Primary Production (NPP) and represents the annual plant growth. Virtually, all of the carbon fixed in NPP is returned to the atmospheric CO_2 pool through two processes: Rh by decomposers (bacteria and fungi feeding on dead tissue and exudates) and herbivores; and combustion in natural or human-set fires.

On longer time scales additional natural fluxes play an important role in carbon balance (thin arrows on the left panel in Figure 1). One of these is the flux of carbon in the form of CaCO3 (dashed lines).The flux of 0.4 PgC/y from atmospheric CO_2 via plants to inert soil carbon is approximately balanced on a time scale of several millennia by export of dissolved organic carbon (DOC) in rivers. A further 0.4 PgC/yr flux of dissolved inorganic carbon (DIC) is derived from the weathering of CaCO3. These DIC and DOC fluxes comprise the river transport of 0.8 PgC/yr. DOC from rivers is respired in the ocean and came back to the atmosphere, DIC is converted in carbonate by marine organism and a part of it is transported as sediment in deep ocean basin. Another fraction returns to the atmosphere.

Processes with longer time scales are burial of organic matter as fossil organic fuel and out -gassing of CO_2 via volcanism processes.

Anthropogenic CO_2 emissions are mainly due to fossil fuel burning and land-use change and affect the natural carbon cycle in various ways (right panel of Figure 1).

The gross amounts of carbon annually exchanged between the ocean and atmosphere, and between the land and atmosphere, represent a sizeable fraction of the atmospheric CO_2 content and are many times larger than the total anthropogenic CO_2 input. In consequence, an imbalance in these exchanges could easily lead to an anomaly of comparable magnitude to the direct anthropogenic perturbation. This implies that it is important to consider how these fluxes may be changing in response to human activities.

CO_2 is taken up by terrestrial ecosystems through several possible mechanisms, for example, land management, CO_2 fertilisation (the enhancement of plant growth as a result of increased atmospheric CO_2 concentration) and increasing anthropogenic inputs of nitrogen. This uptake is limited by the relatively small fraction of plant carbon that can enter long-term storage (wood and humus). The fraction of emitted CO_2 that can be taken up by the oceans and land is expected to decline with increasing CO_2 concentrations. Process-based models of the ocean and land carbon cycles (including representations of physical, chemical and biological processes)

have been developed and evaluated against measurements pertinent to the natural carbon cycle. Such models have also been set up to mimic the human perturbation of the carbon cycle and have been able to generate time-series of ocean and land carbon uptake that are broadly consistent with observed global trends. There are still substantial differences among models, especially in how they treat the physical ocean circulation and in regional responses of terrestrial ecosystem processes to climate. Nevertheless, current models consistently indicate that when the effects of climate change are considered, CO_2 uptake by oceans and land becomes smaller.

1.2 The Greenhouse effect

Even if an increment in CO_2 concentration could influence directly biosphere, the main preoccupation for this enhancing is linked to its role of greenhouse gas.

In Figure 2 is described the mean global radiative balance of the earth. The ultimate source of energy that drives the climate system is radiation from the Sun. About half of the radiation is in the visible short-wave part of the electromagnetic spectrum. The other half is mostly in the near-infrared part, with some in the ultraviolet part of the spectrum. Each square metre of the Earth's spherical surface outside the atmosphere receives an average throughout the year of 342 Watts of solar radiation, 31% of which is immediately reflected back into space by clouds, by the atmosphere, and by the Earth's surface. The remaining 235 Wm−2 is partly absorbed by the atmosphere but most (168 Wm−2) warms the Earth's surface: the land and the ocean. The Earth's surface returns that heat to the atmosphere, partly as infra-red radiation, partly as sensible heat and as water vapour which releases its heat when it condenses higher up in the atmosphere. This exchange of energy between surface and atmosphere maintains under present conditions a global mean temperature near the surface of 14°C, decreasing rapidly with height and reaching a mean temperature of –58°C at the top of the troposphere.

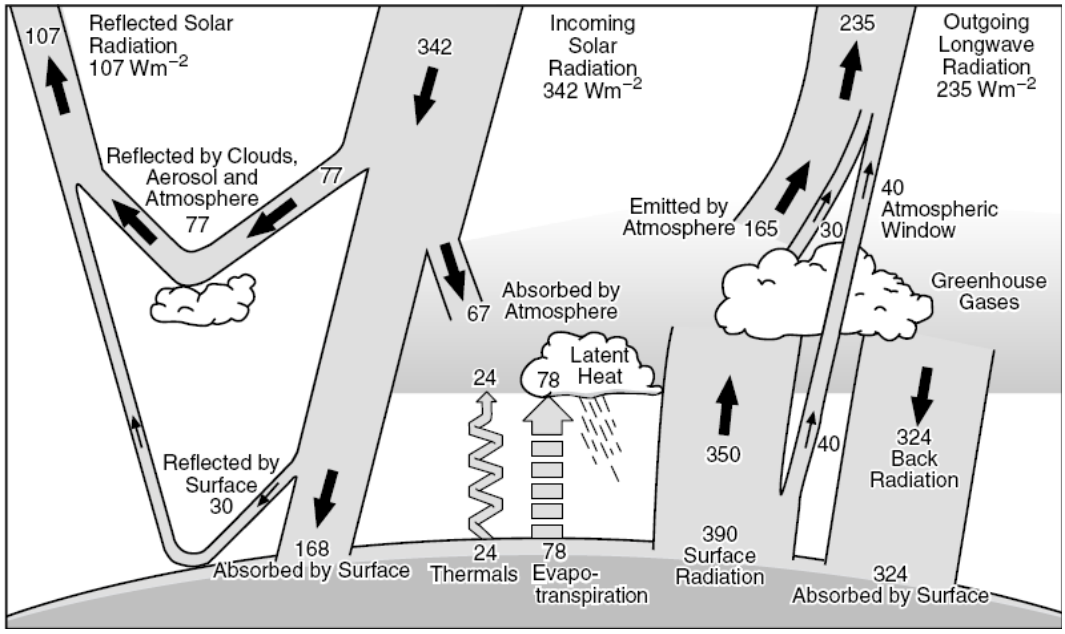

Figure 2: **Global Energy Balance of the Earth**

The major responsible for the absorption of infra-red radiations in the atmosphere are trace gases like CO_2, CH_4, N_2O, CFC and O_3. They emit in turn infra-red radiation in all directions including downward to the Earth's surface. Thus greenhouse gases trap heat within the atmosphere. This mechanism is called the greenhouse effect. The main preoccupation of the scientists is that the enhancement of the greenhouse gas concentrations could cause a return on the earth surface of a larger quantity of emitted infra-red radiation, increasing the earth surface temperature.

CO_2 is not the most effective greenhouse gas, but its concentration is bigger than the others gas, consequently it is the major factor of the total radiative forcing induced by greenhouse gasses. Other greenhouse gasses like CH_4 and N_2O are more effective in trapping CO_2 radiative energy. They could be compared with CO_2 by their "CO_2 equivalent", a measure of the worming potential of each gas compared with CO_2 on a certain period of time, typically 100 years. CH_4 and N_2O have respectively 23 and 296 time the worming potential of CO_2, but their atmospheric concentration are very small.

The effect of worming due to the enhancing of CO_2 concentration led also to important effect on natural feedback between the compartments of carbon cycle. The main consequences are the following:

• Warming reduces the solubility of CO_2 and therefore reduces uptake of CO_2 by the ocean.

• Increased vertical stratification in the ocean is likely to accompany increasing global temperature. The likely consequences include reduced out-gassing of upwelled CO_2, reduced transport of excess carbon to the deep ocean, and changes in biological productivity.

• On short time-scales, warming increases the rate of heterotrophic respiration on land, but the extent to which this effect can alter land-atmosphere fluxes over longer timescales is not yet clear. Warming, and regional changes in precipitation patterns and cloudiness, are also likely to bring about changes in terrestrial ecosystem structure, geographic distribution and primary production.

1.3 The Kyoto protocol

In June 1992 during the United Nation Conference on Environment and Development unfolded in Rio De Janeiro, the countries of United Nation have subscribed same documents about commitments focused on "Sustainable Development", among which the "United Nation Framework Convection on Climate Change (UNFCCC)". With this convection the Countries of United Nation took the commitment to adopt programs and measures addressed to prevention, control and mitigation of the effects of human activity on the planet. In particular, the main goal of the convention is that of "stabilization of greenhouse gas concentrations in the atmosphere at a level that would prevent dangerous anthropogenic interference with the climate system"(art. 2). In December 1997, in Kyoto, has been arranged a Protocol devoted to the actuation of the convention that commits industrialized and developing countries, responsible of the 70% of the world emissions of greenhouse gases, to reduce their emissions of 5.2% than the level of 1990 within 2012. National limitation range from 8% reduction for the European Union and some other to 7% for the United State, 6% for the Japan and 0% for Russia, New Zeeland and Ukraine.

The treaty permitted greenhouse gases increase for Norway(1%), Austria (1%), Australia (7%) and Iceland (10%).

The Kyoto protocol also includes “flexible mechanisms” such as:

- Joint implementation, for the realization between the industrialized countries of common programs in whatever economy sector, finalized to reduction of emissions via the use of more efficient technologies.
- Clean Development mechanisms, for the realization of programs finalized to sustainable development projects that also count high technological and energetic efficiency, executed from industrialized countries in exchange for certified emission shares.
- Emission Trading, that permit to every country to transfer own emission shares or buy it from another country.

Among the measures adopted by Kyoto protocol there is the commitment of the parties (Annex1 countries) to inventory both sink and source of greenhouse gas. Article n° 4 of the protocol prescribe that “All Parties shall develop, periodically update, publish and make available to the Conference of the Parties, national inventories of anthropogenic emissions by sources and removals by sinks of all greenhouse gases not controlled by the Montreal Protocol, using comparable methodologies to be agreed upon by the Conference of the Parties”.

Moreover is scheduled the implementation of a national system for the estimation of anthropogenic emissions by sources and removals by sinks of all greenhouse gases.

In 1988, the World Meteorological Organization (WMO) and the United Nations Environment Programme (UNEP) co-established the Intergovernmental Panel on Climate Change (IPCC). One of the IPCC’s activities is to support the UN Framework Convention on Climate Change (UNFCCC) through its work on methodologies for National Greenhouse Gas Inventories. The last report of IPCC about emission inventory was published in 2006 the revised version of the IPPC Guidelines for IPCC Greenhouse Inventory. This work was born to assist countries in compiling complete, national inventories of greenhouse gases. The guidance has

been structured so that any country, regardless of experience or resources, should be able to produce reliable estimates of their emissions and removals of these gases. In particular, default values of the various parameters and emission factors required are supplied for all sectors, so that, at its simplest, a country needs only supply national activity data. The IPCC also manages the IPCC Emission Factor Database (EFDB). The EFDB was launched in 2002, and is regularly updated as a resource for inventory compilers to use to assist them by providing a repository of emission factors and other relevant parameters that may be suitable for use in more country-specific methodologies.

IPCC Third Assessment Report (hereafter TAR) clarifies the factors that induce climate to change over a wide range of time scales and our capability to simulate the behaviour of climate system under different forcing scenarios.

The major areas where advances in science of climate system have been made are:

- Observational research (atmospheric, marine and terrestrial) aimed at a better quantification of carbon fluxes on local, regional and global scales. For example, improved precision and repeatability in atmospheric CO_2 and stable isotope measurements; the development of highly precise methods to measure changes in atmospheric O_2 concentrations; local terrestrial CO_2 flux measurements from towers, which are now being performed continuously in many terrestrial ecosystems; satellite observations of global land cover and change; and enhanced monitoring of geographical, seasonal and inter-annual variations of biogeochemical parameters in the sea, including measurements of the partial pressure of CO_2 (p CO_2) in surface waters.
- Theory and modelling, especially applications of atmospheric transport models to link atmospheric observations to surface fluxes (inverse modelling) the development of process-based models of terrestrial and marine carbon cycling and programmes used to compare and test these models against observations; and the use such models employed to project climate feedbacks on the uptake of CO_2 by the oceans and land.

TAR highlighted same broad range where science should direct the attention to limit the uncertainty that still limits the ability to understand, detect and predict climate change. One of this is the necessity to expand the available observational data to provide long-term records with increased temporal and spatial coverage.

At a broad scale, inverse model techniques were able to estimate global CO_2 flux starting from concentration measurement in the atmosphere, taking to useful indications about the size of the exchange at a global or at least continental scale. The localization of source and sink at a detailed scale is still limited. There is the necessity in understanding exchange mechanism at intermediate scale over areas more heterogeneous from a bio-geophysical and morphological point of view (Gioli et al, 2007).

Chapter 2: The Planetary Boundary Layer

The earth surface is a boundary on the domain of the atmosphere. Transport process at this boundary modifies the lowest 100 to 3000 m of the atmosphere, creating what is called Planetary Boundary Layer (PBL) or simply Boundary Layer (BL). As defined by Stull, 1998 this layer is the part of the troposphere that is directly influenced by the presence of earth's surface and responds to surface forcings with a timescale of about an hour or less. Surface forcings include the fractional drag, evaporation and transpiration, heat transfer, pollutant emission, and terrain induced flow modification (Stull, 1998).

Turbulence is one of the most important features in the PBL and it can be associated with thermal convection and mechanically (shear induced by the friction).

2.1 Convection and atmospheric stability

The vertical transport of momentum, heat, moisture and pollutants from the surface to the higher levels of the atmosphere is mainly due to turbulent convention. A major control on the type and extent of convective activity is the vertical temperature structure as expressed in the concept of stability.

A parcel of air moving up through the atmosphere is said to moving adiabatically if neither gives or receives heat from surrounding air. As it rises it encounters lower atmospheric pressure because the mass of air above it became progressively less. Internal pressure of the parcel increases and it tends to expand. To push away the surrounding air requires work and therefore energy. But the only energy available is the thermal energy of the parcel itself (assuming any exchange with the surroundings), thus as the air parcel rises it cools. In dry unsaturated air the rate of temperature change, namely the rate of such a parcel with height is called dry adiabatic lapse rate (Γ). The unsaturated air condition is valid in about all the application presented in this work.

Instead, environmental lapse rate ($\frac{\partial T}{\partial z}_{env}$) is the actual decrease in temperature with an increase in altitude through the atmosphere. It represents the rate at which a dry parcel will cool or worm if it is moved respectively upward or downward through the atmosphere.

Atmospheric stability is the relative tendency for an air parcel to move vertically. It can be evaluated comparing with. There are tree possibilities:

- If $\frac{\partial T}{\partial z}_{env}$ is greater than Γ an air parcel is pulled further away from its starting point by buoyancy (its temperature is always higher than the environmental air). The atmospheric layer is said to be **statically unstable**. Unstable region are turbulent.
- If $\frac{\partial T}{\partial z}_{env}$ is smaller than Γ. In this case a displaced air parcel always finds itself colder than the environment air and then tends to sink back. This situation defines a **stable** atmospheric layer. Namely it is smooth and non-turbulent.
- If $\frac{\partial T}{\partial z}_{env}$ is equal to Γ it means that air parcel has a temperature equal to the surrounding environment and there is any tendency for the air parcel to rise or sink. The air of environment is called **statically neutral**.

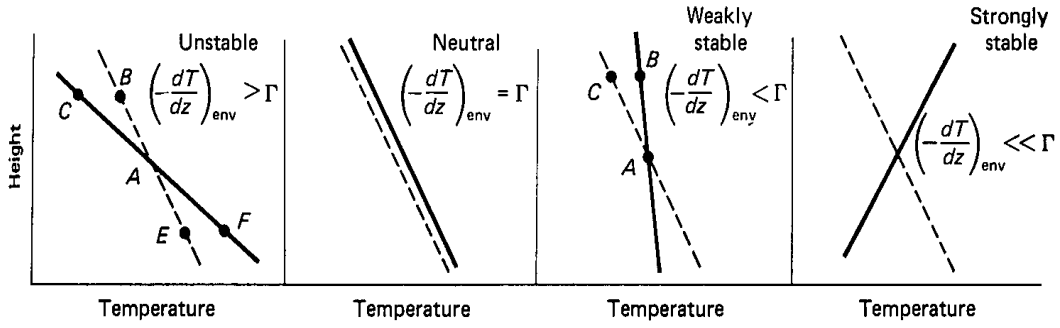

Figure 3: ***Description of four cases of atmospheric stability***

When considering atmospheric stability it is often useful to use potential temperature (Θ) instead of the observed air temperature. The potential temperature of a parcel is the value it would have if it were at the arbitrary pressure value of 100 kPa. This is

because the main goal is to compare air parcel existing at different pressure level, then it's useful to standardize conditions to a common pressure.

2.1 Diurnal evolution of PBL

The planetary boundary layer is continually evolving in response to the daily heating /cooling cycle and to changing synoptic conditions. The temporal dynamics of the boundary layer under "ideal" weather condition are illustrated in Figure 4.

The PBL height waxes and wanes between its lowest typical value of the order of 100 m (range 20–500 m) in the morning to the highest value of the order of 1 km (range 0.2–5 km) during late afternoon (Arya S.P., 2005). Mean winds, temperatures, and other properties, as well as turbulent fluxes also exhibit strong diurnal variations. Diurnal variations of the PBL height and other properties are found to be considerably smaller or almost absent over large lakes, seas and oceans, as well as over high latitude land areas during winter.

In Figure 4 is shown schematically the stratification of the lower atmosphere during a diurnal cycle, and the evolution in time of ABL.

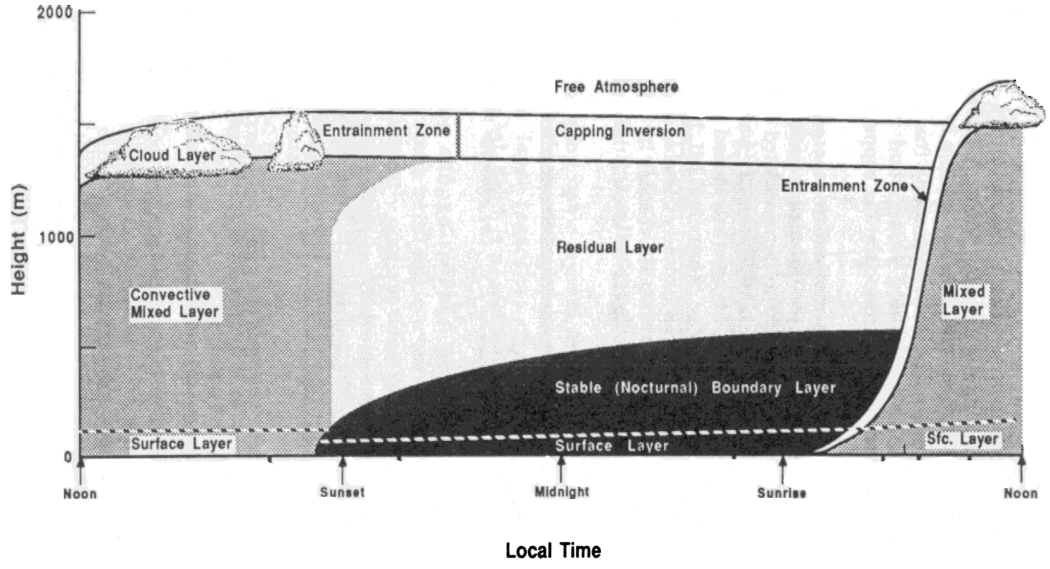

Figure 4: ***Diurnal evolution of the Planetary Boundary Layer***

During the daytime has been observed the formation of a Convective Boundary Layer (CBL), where the turbulence grows in depth. It is capped by a statically stable entrainment zone of intermittent turbulence. The CBL is characterized by intense mixing in statically unstable situation where thermals of warm air rise from the ground, reaching a maximum in depth in late afternoon. The resulting turbulence tends to mix heat, momentum and moisture uniformly in the vertical. At sunset, the radiative cooling of the ground leads to a shallow Stable Boundary Layer (SBL). Turbulence also decays, leaving a residual layer in the place of the mixed layer. Finally, after sunrise the CBL develops again destroying the SBL. In the absence of significant cooling or heating the PBL tends to become a Neutral Boundary Layer (NBL). This work is referred to such case studies of Convective Boundary Layer situations.

2.1.1 The Convective Boundary Layer

In the Convective Boundary Layer the turbulent flow is mainly driven by buoyancy. In a CBL, warm rising air from the surface organizes itself into thermal plumes or eddies, that can occupy substantial areas (diameters of up to 1 km) and reach the top of the boundary layer. These plumes mix air from the surface to the top of boundary layer very effectively, and thereby create a very well mixed layer. As result quantities like heat and moisture remain almost constant with height and the vertical gradient is approximately constant in time.

In Figure 5 are shown ideal vertical profiles of scalars and kinematic fluxes during daytime.

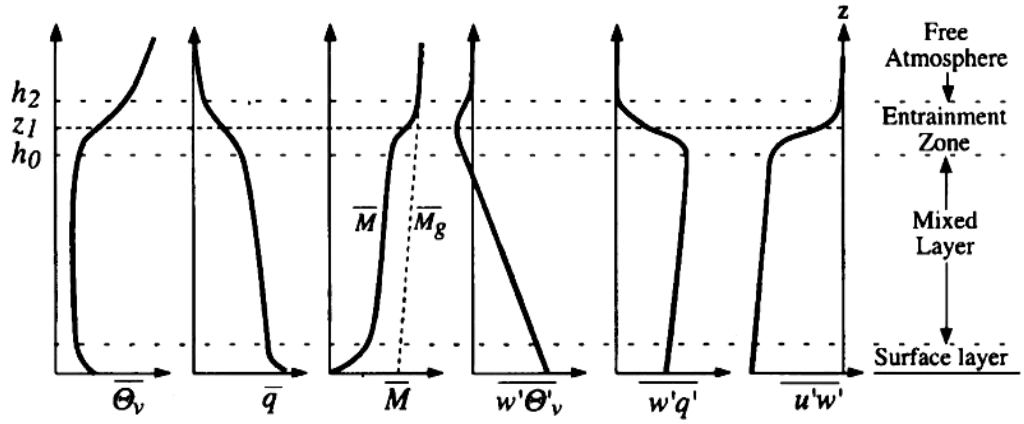

Figure 5: ***Vertical profiles of scalars and mass and energy fluxes in an ideal CBL***

2.2.2 Boundary Layer height estimation

The strategies adopted in this work that owing to approximately determine the height of the BL are based on a careful examination of experimental data, taking into account the different "PBL height" definitions , selected between methods suggested in literature (*Sullivan et al., 1998; Stull, 1998; Arya S.Pal, 2005*).

Gradient method. This method defines the BL height as the vertical location where the Potential Temperature gradient reaches its maximum value. Approaches concerning lapse rate criteria to identify the thermal inversion were developed by *Heffter* and reviewed by other authors (*Kienele et al, 1985*). Original Heffter definition identified the height *H* as the quote *z* where the Potential Temperature vertical gradient is greater than 0.5°K /100 m.

Other quantities sampled over vertical profiles could be used to estimate the mixing height. For instance, BL height could be defined by a rapid decrease in humidity, a shear wind increment or a sudden change in gas concentrations profiles.

Flux method. Deardorff et al. (1980) define the entrainment zone as the layer where the sensible heat flux becomes first negative and then vanishes. In this definition the BL height is placed at the location of the minimum average heat flux.

TKE method. Turbulent Kinetic Energy is a key variable in describing surface land-surface processes because it is a measure of turbulence intensity and is directly related to momentum, heat and moisture transport through the Boundary Layer. The method introduced by *Seibert et al.* (2000) locates the mixing height at the altitude where the TKE is reduced by 5% with respect to its maximum value inside the Boundary Layer.

2.2 *Entrainment and subsidence*

In the following it will be applied a methodology in which the estimation of the vertical transport on the top of the mixed layer is required. Basing on the nature of the motions it's possible to distinguish two types of processes driving transport above the entrainment zone: entrainment and subsidence.

Turbulent structures from the CBL could penetrate temporarily into the layer above until their upward momentum is reversed by stable stratification there. By this process air from free troposphere could enter in the CBL and mixes. The net flux from the free atmosphere to the CBL is called entrainment flux.

One of the effects due to this process is to enrich or the CBL CO_2 content because air with a different concentration is drown down into the mixed layer. Another effect is to change the vertical extent of CBL. The entrainment flux is turbulent by nature. It is by definition a flux though a moving surface and not though a surface fixed in space (Laubach et al, 2002). The entrainment process is described by a velocity w_e (the entrainment velocity) that represents the spatial average of vertical speed of air on the top of the CBL.

The vertical air movement balancing the horizontal mass divergence caused by synoptic pressure gradients is called “subsidence”. The name indicate that the motion is normally expected downward ($w<0$), as in the case of anticyclonic systems, which are most likely to produce an undisturbed growing CBL at daytime. Subsidence enhances the amount of air entrained from above without increase the height of well mixed column. This is possible because at the same time air from inside the column diverges sideways. Subsidence process consist in an imbalance between the

additional inflow from above and the outflow to the sides, thus a net flux of , which it is called subsidence flux. Conversely, if there is convergence and a rise of air (w>0), then the "negative subsidence" flux expresses the imbalance between inflow through the sides and reduced inflow from above (Laubach et al, 2002).

2.3 Effect of the spatial in homogeneity: sea breeze

In the real world relatively few surfaces are flat and homogeneous. Each field of a landscape possesses its own combination of radiative, thermal, moisture and aerodynamic properties, such as albedo, soil conductivity, soil moisture, surface roughness, etc. The differences are manifested as different surface and atmospheric climate in terms of temperature, humidity and wind speed profiles (Oke, T.R., 1978). At the boundary of the different surfaces these gradients are great and horizontal interactions occur.

Then, these situations are also observed whenever there is an interface between water (sea or lake) and land. These two different surfaces possess contrasting thermal responses because of their different properties and energy balances. Compared with most land surfaces a water body exhibits very little diurnal change in surface temperature. Water is different because allows transmission of short-wave radiation to considerable depths, is able to transfer heat by convection and mixing, converts much of its energy into latent rather than sensible heat, has a large latent inertia due to its higher heat capacity. The reduced sensible heat fluxes over water bodies means that atmospheric warming and cooling rate are relatively small. In contrast the convective fluxes and rate of temperature change over land are large and shows a diurnal variation. The land/water differences and their diurnal reversal produce corresponding land water air pressure differences. These in turn result in a system of breezes across the shoreline which reverses their direction between day and night. In the morning, the great sensible heat flux density over land heats the air column more rapidly and to greater heights than over the water. This result in a flow at upper levels towards the water, in so doing it must produce grater pressure at the surface over the water and hence a cross shoreline flow develops from water to land (Figure 6). Stronger winds could modify these types of local winds.

Land and sea breeze is only the low level portion of the complete circulation cell.

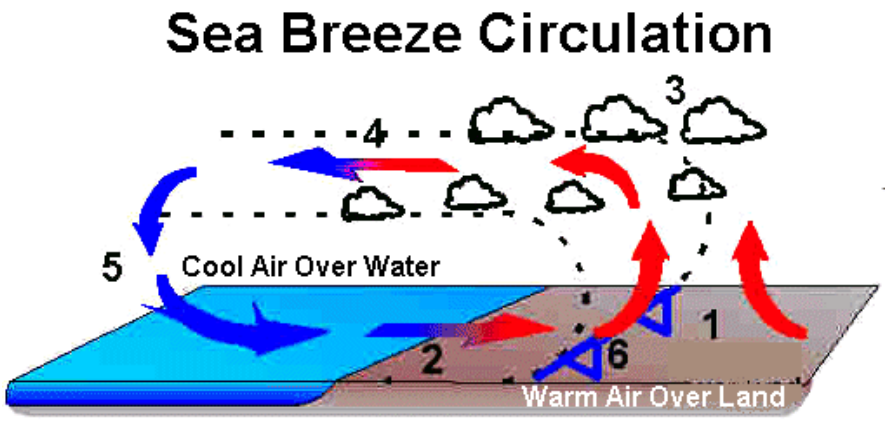

Figure 6: ***Typical sea breeze circulation cell***

Some of the component of the sea breeze system is the following (Miller et al, 2003):

- Sea Breeze Circulation is a vertically rotating cell, with shoreward flow near Earth's surface, rising air currents inland, diffuse sinking currents several kilometres out to the sea, and usually seaward return flow near 900 hp;
- *Sea Breeze Gravity current* is the landward flow of cool, moist marine air in the lower horizontal harm of SBC;
- *Sea Breeze Front* (SBF) is the landward edge of the SBG and the SBC, often associated with sharp changes in temperature, moisture, and wind. Its approach may be marked by development of fair weather cumulus clouds;
- *Kelvin Holtzman Billows* are the waves that develop along the upper boundary of the SBG during period of low static stability (midday).
- *Convective Internal Boundary Layer* (CIBL) is an instable region within the marine air mass, appearing at the coast and growing in depth with distance inland. In it pollutant could be trapped and concentrated.

The advancing sea breeze front produces uplift in what is already an unstable atmosphere over the land.

The sea breeze phenomena have been studied because of an important pollutant phenomena occurring in these atmospheric conditions: the fumigation process. In Figure 7 is shown what happen when a shoreline source is emitting effluent into the stable air of the offshore portion of a sea breeze. The associated fanning plume drift inland until it encounter the developing unstable boundary layer of the warmer land at which point it fumigates. The resulting mixture is advected further inland and sea breeze front is advected as a "wall of smoke" (Figure 7).

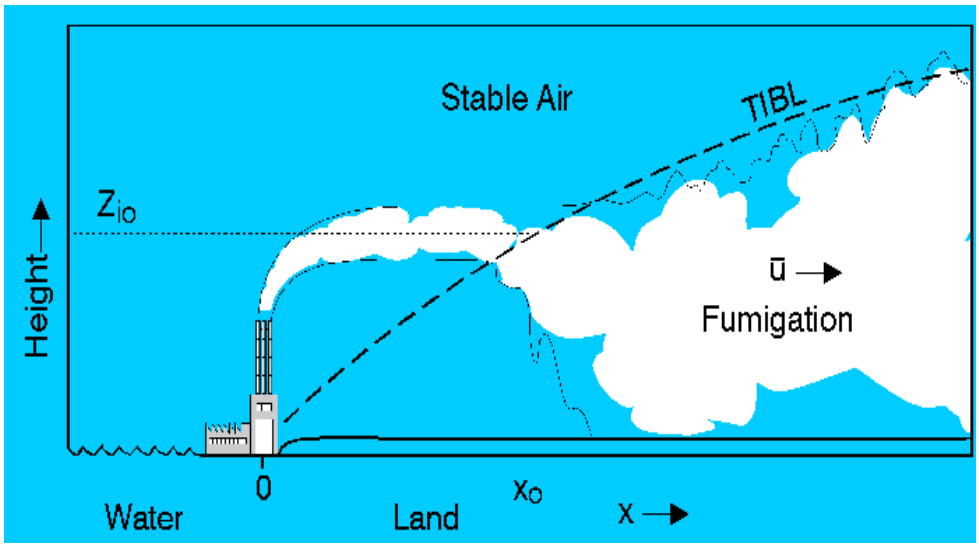

Figure 7: Illustration of coastal fumigation.

Chapter 3: The SkyArrow ERA aircraft

The possibility to use small aircraft for measuring surface mass and energy fluxes was demonstrated in a large number of pilot experiments over the past decade. In particular, the scientists of NOAA have shown that aircraft flux measurements can be very accurate and reliable and still be executed on small lightweight aircraft. Critical in the development of this type of aircraft is its capability to fly at low altitude and low speed, thereby allowing comparisons between flux estimates from ground sites and from the aircraft, and allowing to make flux estimates at high spatial resolution.
Sky Arrow ERA (Environmental Research Aircraft) has been developed to host the Mobile Flux Platform (MFP) which consists of a set of sensors for atmospheric measurements (Figure 8).

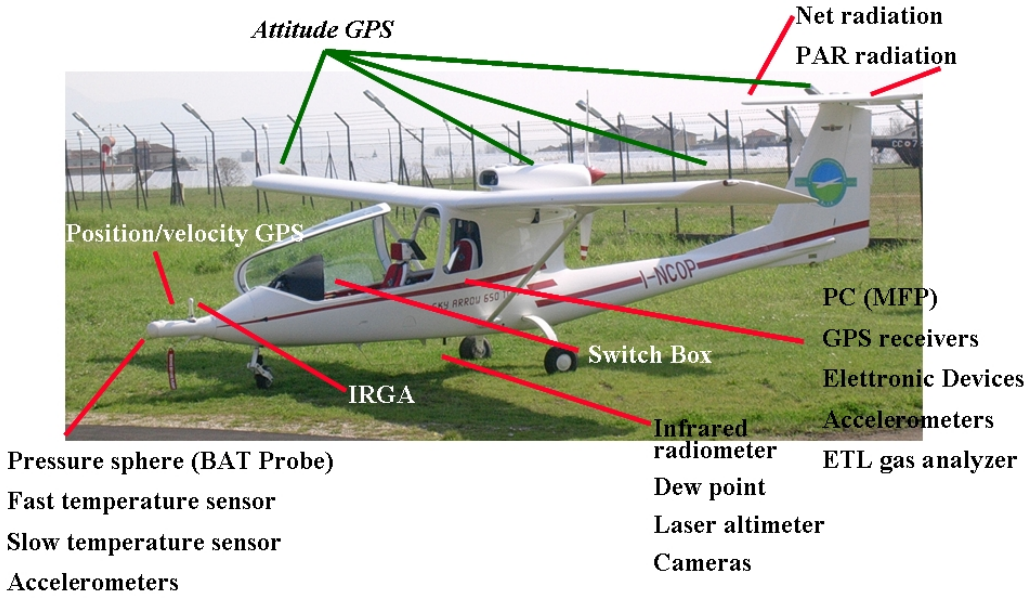

Figure 8: Sky Arrow ERA with sensors and instruments mounted

The pusher engine configuration is ideal for turbulence measurements, because it allows instruments to be mounted on the nose of the fuselage where they can project into the relatively undisturbed air ahead of the aircraft. In addition, the high wing configuration results in a high vertical separation between the probe and the wing, minimizing flow distortion effects in the probe region due to air circulation around the wing, the so called 'upwash' effect (Crawford et al., 1992). With its clean

aerodynamics due to the pusher configuration, the Sky Arrow is thus able to perform low-and-slow air-surface-exchange measurements.

3.1 The Mobile Flux Platform (MFP)

The MFP computer is purchased from off-the-shelf components to aid in replacement and troubleshooting if any part of the computer should fail in service. The computer itself consists of a single-board computer and industrial chassis from American Portwell Technologies. Two PCI serial cards from Quatech and a custom ISA card finish the system.
Following the main characteristics:

Best Aircraft Turbulence Probe (BAT) The BAT probe assembly is a system of circuit boards and electronic hardware encased in a weatherproof fiberglass/carbon fiber housing that is mounted on the nose of an aircraft.

Figure 9: The bat probe

The probe assembly consists of a pressure sphere with 9 holes used to measure the magnitude and direction of the incident wind vector on the hemisphere. A tapered cone after body houses a BAT-REM module that is used for digitizing the analogical signals and providing a serial data stream to the host MFP computer, much like the BAT-REM module in the auxiliary box. In addition to pressure measurements, a set

of three orthogonal accelerometers is also installed in the pressure sphere to measure high frequency motion of the hemisphere in three dimensions. High and low frequency air temperature measurements are made utilizing a PRT probe and a micro-bead thermister. Static pressure measurements from the pressure sphere round out the BAT probe instrument suite.

Laser altimeter: Riegl Ld90-3: This is a laser range finder that is mounted so that is looks downward from the bottom of the aircraft. The laser reports distance at programmable time intervals (up to 100 Hz) via an RS-232 serial port. Data is acquired through one of the eight serial ports on the Quatech ESC-100-D9 eight-port serial card in the MFP computer. An electrical pulse generator periodically drives a semiconductor laser diode sending out infrared light pulses, which are collimated by the transmitter lens. Via the receiver lens, part of the echo signal reflected by the target hits a photodiode which generates an electrical receiver signal. The time interval between the transmitted and received pulses is counted by means of a quartz-stabilised clock frequency. The calculated range value is fed into the internal microcomputer which processes the measured data and prepares is for range (and speed) display as well as for data output.

Accelerometers (ICSensors), The accelerometer consists of a silicon micro machined accelerometer with signal conditioning electronics in a lightweight Valox™ housing that can be easily attached to a mounting surface. On the aircraft are mounted two three dimensional set of accelerometers, on the nose of the aircraft and in the back seat in the auxiliary box near the centre of gravity.

Satellite position systems:

Position GPS: Novatel RT-20: the NovAtel OEM4-G2 RT-20 GPS system is used to measure the position and velocity of the aircraft using differential corrections at 10 Hz. The antenna for this system is mounted on the top of the BAT probe assembly. Data is acquired through one of the eight serial ports on the Quatech ESC-100 eight-port serial card in the MFP computer.

Attitude GPS: Javad. Javad AT4 GPS attitude system is used to measure the pitch, roll, and heading angle of the aircraft with respect to Earth at 20 Hz. The system utilizes four antennas to make its attitude measurement. The first antenna is mounted on top of the Sky Arrow just behind the cabin. The second is mounted on top of the vertical fin and horizontal stabilizer. The third is mounted on top of the left wing near the wing/strut junction, and the fourth is mounted on top of the right wing near the wing/strut junction. Data is acquired through one of the eight serial ports on the Quatech ESC-100 eight-port serial card in the MFP computer.

Open-Path Analyzer IRGA Licor-7500:

The LI-7500 is a high performance, non-dispersive, open path infrared CO_2/H2O analyzer designed for use in eddy covariance flux measurement systems. Some of the LI-7500's important features include:

- Simultaneous measurements of CO_2 and H2O in the free atmosphere.
- High speed measurements. Internal 150 Hz measurements are digitally filtered to provide a true 5, 10, or 20 Hz bandwidth.
- Withstands exposure to rain or snow without damage or calibration shift.

EdgeTech 200 DewTrack (Tdew): The model 200 DewTrack® Humidity transmitter is a low power, blind transmitter which consists of a sensor probe and an electronic control unit. The control unit is housed in a plastic or aluminium enclosure. This instrument combines the inherent accuracy, reliability, and long term stability of optical chilled mirror technology with an advanced electro-optic sensing scheme. The model 200 provides continuous and repeatable humidity measurements.

Radiation Energy Balance Systems (REBS) Q*7: The Q7 is an high-output thermopile sensor that generates a millivolt signal proportional to the net radiation level, that is the algebraic sum of incoming and outgoing all-wave radiation (i.e. short-wave and long-wave components). Incoming radiation consists of direct (beam) and diffuse solar radiation plus long-wave irradiance from the sky. Outgoing

radiation consists of reflected solar radiation plus the reflected long-wave component. The sensor is mounted in a glass-reinforced plastic frame with a built-in level. A ball joint is supplied on the stem to facilitate levelling. The sensor surface and surrounding surfaces are painted flat black to reduce reflections within the instrument and to achieve uniform performance over reflective and non-reflective surfaces. Sensor surfaces are protected from excessive convective cooling by hemispherical polyethylene windshields. Polyethylene is used for the windshield material because it is transparent to both long and shortwave energy. The windshields are open to the atmosphere through a desiccated breather tube to prevent the domes from collapsing at night. A mounting stake located away from the tower to decrease shading and interference is recommended. Net radiation measurement height is typically between 1 and 3 m.

Figure 10: The Net Radiation sensor

Licor 190SA: During photosynthesis, plants use energy in the region of the electromagnetic spectrum from 400-700 nm. The radiation in this range, referred to as Photosynthetically Active Radiation (PAR), can be measured in energy units (watts m-2) or as Photosynthetic Photon Flux Density (PPFD), which has units of quanta (photons) per unit time per unit surface area. The units most commonly used are micromoles of quanta per second per square meter (mmol s-1 m-2).

Figure 11: PAR radiation sensor

Chapter 4: Methods for the estimation of surface mass fluxes at territorial scale

Quantifying trace gas emissions and the influence of surface exchange processes on the atmosphere is a necessary step towards the control of global greenhouse gas emissions and reliability of air quality models.

Several methodologies exist in literature that are used to assess calculation of surface fluxes of carbon dioxide.

The "Airborne eddy covariance" is a useful technique to directly measure surface energy, mass and momentum fluxes at the regional scale. Its accuracy and reliability has already been assessed in literature (Crawford et al, 1996).

The coupling of the Airborne Eddy Covariance calculation over a box with the estimation of vertical divergence of the flux allow its extrapolation at surface level. Eddy correlation is the base concept for the "Low level flight + Inverse method" (Bunge et al, 2006) that, till now, have been used successfully for both water vapour and energy fluxes estimation. Preliminary results applying the method for carbon dioxide fluxes are reported in this work.

A further method is the "CBL budget" that exploit the well mixed properties of the Convective Boundary Layer and the principle that variation in time of gas concentration inside the Boundary layer reflect the surface flux (Cleugh et al 2004, Laubach at al 2002, Schmitgen et al 2004):

One of the uncertainness regarding the validity of the method in these kind of applications is connected to the shortage of ideal meteorological condition during the experiments, above all because, in such case, the advection could play an important role (Lloyd et al., 2001, Laubach and Fritsch, 2002, Styles et al., 2002, Cleugh et al., 2004, Schmitgen et al., 2004). Also, both surface heterogeneity and topographical effects could create local advective fluxes leading to increasing uncertainty in resulting surface fluxes.

In this chapter a different mass balance approach is reported, where the surface fluxes are inferred starting from known fluxes measured on the lateral face of an air

volume (Wratt et al, 2000, Kalthoff et al, 2002). This is the most affective approach when the study is focused on fluxes estimation over coastal terrains, where sea breeze effect does not permit to neglect advection. Sea breeze inlet from the sea is poor in CO_2 and allows obtaining important gradients between the measured in-flux and out-flux of an air volume.

To integrate both in and out-fluxes over the lateral surfaces of the ideal cubic portion of atmosphere, two different interpolation approaches have been evaluated. Shepard method application has been implemented in collaboration with the Institute for the Application of Calculation "Mauro Picone" of Naples. Bayesian Markov Chain Montecarlo method was also adopted, in collaboration with "Parthenope" university of Naples.

4.1 Airborne Eddy Covariance

The Eddy Covariance is a well established method that allow calculating turbulent fluxes of both mass and energy. The method is based on the measurement of the turbulent motion of the air that is the carrier for the mass and energy.

Direct calculation CO_2 mass fluxes via eddy covariance is based on high frequency measurements of wind velocity and concentrations of the scalar. CO_2 flux by eddy covariance technique is given by:

$$Fc = \overline{w\rho_c} = \overline{w'\rho_c'} + \overline{w}\,\overline{\rho_c} \qquad (4.1)$$

Where w is the vertical wind velocity and ρ_c is CO_2 density. The prime indicates the fluctuation as deviations from the mean value (overbar) over a sampling period.

The first term on the right side of equation 4.1 is the turbulent flux; the second term represents the CO_2 flux due to the mean vertical flow. This term is included in our calculations applying the Webb correction (Webb et al, 1980) exposed in section 4.1.1.

Fluctuations of the quantities in equation 4.1 are referred to the mean calculated over an opportune time interval T. Time interval on which mean and covariance are calculated have to be long enough to sample all turbulent structures responsible for the transport of the scalar. Moreover it hasn't to be too long because it's necessary to

fulfil steady state conditions. Ground measurements usually require an interval of 30 minute.

Airborne eddy covariance has same differences that respect to eddy correlation applied at a ground station.

Since aircraft are faster than the air flow, in airborne eddy covariance application the sampled turbulent structures are grater than those sampled in the tower based eddy covariance. For this reason the sampling frequency have to be higher (50 Hz against 20 Hz). As consequence the time period over where the covariance is computed is less than the "30 min" commonly used in the tower based measurement, typically of the order of few minutes (Gioli et al, 2007).

Statistics calculated by Airborne Eddy covariance technique are not necessarily based on Taylor hypothesis of *frozen turbulence* (Taylor , 1921), that instead is at the base of the ground based measurement. A flux measured by Airborne eddy covariance is an instantaneous view of turbulent structure in the space. "Spatial length" on which covariance is calculated have to be broad so as to include low frequency contributes to the fluxes but at the same time it cannot be too much large running the risk to have a low spatial resolution of fluxes and non steady state conditions. This parameter is dependent by roughness on the surface, atmospheric stability and flight altitude and the "best length" in usually found using spectral analysis.

4.1.1 Webb correction

Webb *et al*. (1980) suggested that the flux due to the mean vertical flow cannot be neglected for trace gases such as water vapour and CO_2. To evaluate the magnitude of the influence of the mean vertical flow, Webb *et al*. (1980) assumed that the vertical flux due to the density fluctuation of the dry air (ρ_a) should be zero:

$$\overline{w\rho_a} = \overline{w}\,\overline{\rho_a} + \overline{w'\rho_a'} = 0 \qquad (4.2)$$

Using the ideal gas equation, the final expression for the mean vertical flow is:

$$\overline{w} = \frac{\mu}{\overline{\rho_a}}\overline{w'\rho_v'} + (1+\mu\sigma)\frac{\overline{w'T'}}{\overline{T}} \qquad (4.3)$$

The total CO_2 flux is:

$$Fc = \overline{w'\rho_c'} + \mu\frac{\overline{\rho_c}}{\overline{\rho_a}}\overline{w'\rho_v'} + (1+\mu\sigma)\frac{\overline{\rho_c}}{\overline{T}}\overline{w'T'} \qquad (4.4)$$

Where μ is the ratio of the molecular weights of dry air and water vapour, σ is the ratio of water vapour and dry air densities, ρ_v is the water vapour density and T is the absolute temperature.

4.2 Low level flight with Inverse method

The "Low Level Flight with Inverse Model" is a method developed by Bunge et al. (2004) using a combination of Low Level Flight (LLF) and inverse model theory (IM) in order to derive area average turbulent flux over a determinate area. The LLF method determines the surface fluxes from flights at only one low flight level by solving the budget equation. Inverse model is used in order to derive horizontal gradients and temporal development of the scalars and wind.

The advantage of the method is that it's able to determine the area average turbulent fluxes using just one low level flight pattern.

Surface flux is obtained using a linear extrapolation to the ground:

$$Fs = F_{fl} - \frac{\partial F}{\partial z}z \qquad (4.5)$$

(Where the subscript fl and s represents respectively the level of flight and surface, F is the flux of the scalar and z the altitude); then it works well only if the vertical profile of the turbulent flux of the scalar has a linear shape (as observed in a typical CBL).

In the original form of the methodology the values F_{fl} is measured at first by applying eddy correlation over the single legs and then averaging the results over the entire low level flight pattern. Quantity $\frac{\partial F}{\partial z}$ was estimated separately by inverse model. A little variation is done in this work since the surface flux is estimated at first extrapolating surface fluxes at each measurements point and then averaging them over the entire flight pattern.

Moreover, until now method was adopted for the estimation of Latent and Heat turbulent flux (Bunge et al, 2006). In this thesis a tentative in using the method is

done to estimate CO_2 turbulent flux. The flux at flight level is calculated averaging the punctual fluxes measured over the whole lowest flight pattern.

A Bayesian inverse model is used to estimate horizontal and vertical gradients of the scalar terms of the continuity equation in order to calculate vertical divergence of the flux (the term $\frac{\partial F}{\partial z}$).

Considering we want to calculate CO_2 vertical divergence we have to estimate the following equation:

$$\frac{\partial F_{co2}}{\partial z} = -\frac{\partial co_2}{\partial t} - \vec{\bar{U}} \bullet \quad grad\, co_2 \qquad (4.6)$$

For the inverse modelling (Bange et al, 2006) an input of the CO_2 mixing ratio and the wind vector for at least one flown box must be given as a function of time and 3D position. The model then works with a linear assumption for the mixing ratio c of the CO_2 with the parameters m0, m1, m2, m3 and m4 and the position (x, y and z) and time t:

$$CO_2 = m_0 + m_1 \cdot x + m_2 \cdot y + m_3 \cdot z + m_4 \cdot t. \qquad (4.7)$$

The parameter m_0 is a constant mean CO_2 mixing ratio while m_1, m_2, m_3, m_4 represent the directional and temporal derivations of the mixing ratio:

$$m_1 = \frac{\partial co_2}{\partial x};\ m_2 = \frac{\partial co_2}{\partial y};\ m_1 = \frac{\partial co_2}{\partial z};\quad m_1 = \frac{\partial co_2}{\partial t} \qquad (4.8)$$

To start the model, some a priori assumptions on physically logic basis must be given for the deviations of the mentioned parameters and for the accuracy of the measurement equipment (LICOR 7500).

4.3 "Fixed Volume" Mass Balance Method

The CBL budget technique is based on the conservation of the mass equation integrated over a defined volume of air. A traditional choice for that volume is a column with the earth surface as the bottom ($z = 0$) and the CBL height as the top ($z = z_i$), which is considered a natural choice since z_i separates flow regimes, and turbulent fluxes above it are largely inhibited (Laubach et al, 2002).

Lateral sides of the virtual volume intersect the locations at which vertical concentrations and wind are measured by aircraft. Once a virtual box is defined, the budget i.e. sinks and source at the earth surface like vegetation, soil industries etc... (arrow n°3 in Figure 12) could be estimated via the evaluation of the following terms:

- vertical turbulent transport of the gas thought the box (arrow n°1)
- horizontal turbulent transport of gas thought the sides of the box (arrow n°2)
- vertical advection of the gas in the volume due for instance to subsidence (arrow n°4)
- horizontal advection of the gas in the volume due to mean wind (arrow n°5).

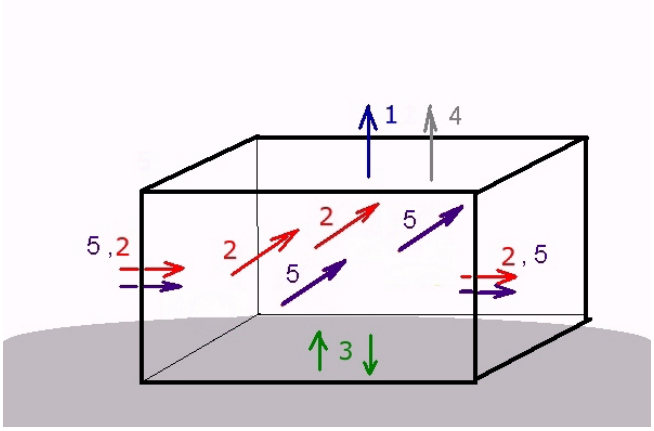

Figure 12: Representation of the main fluxes through an air volume

In this study instantaneous surface fluxes of CO_2 has been calculated on the basis of aircraft measurements sampled into the BL at several altitudes. The implementation assumes that all measurements are taken at the same time as to have a snapshot picture of the air column. As a result it's indirectly possible to assume no chemical reaction of the gas, constant emission and constant BL height (or TIBL height). This implies that measurements have to be taken during the afternoon hours, a time interval at which meteorological conditions could be assumed constant. The assumption that CO_2 does not react chemically at the spatio-temporal scales of the study presented here is well-justified, since gas fluxes are evaluated at the scale of about 1 hour and 25 Km^2.

A further simplification in the model is to neglect turbulent fluxes in the horizontal direction, which are very small in comparison with horizontal advection.

Some problems occur in the implementation of the model:

- Aircraft does not describe straight patterns, so that virtual surfaces of the air column are not correspondent with the spatial location of sampled data. Moreover data have to be interpolated over the entire surface of the considered volume to integrate horizontal fluxes.
- Fluxes have to be also inferred for the top surface of the virtual box where also turbulent fluxes could be important and need to be estimated. This task is complicated by the difficulty in performing direct measurement exactly over the entrainment layer.

In order to estimate top surface fluxes we have to distinguish two different conditions, one for the estimation of turbulent fluxes and the other for transport due to mean horizontal wind.

To calculate the trace gas transport thought the ceiling of the control volume, the mean vertical wind at the upper edge of the air volume is determined by vertically integrating the continuity equation with, as boundary condition, zero vertical velocity at the ground surface:

$$\overline{w} = -\frac{1}{\overline{\rho} A_T} \sum_k \sum_{i,j} \rho_{i \cdot j.k} (\underline{q} \cdot \underline{n})_{i,j,k} \Delta s_{i,j,k} \qquad (4.9)$$

Where ρ is air density and denotes mean value on the upper surface; A_T is the area of the upper surface and i, j, k indexes refer to horizontal and vertical coordinates of any grid cell. Then the approximated flux through this surface is given by

$$F_{CO2,top} = \overline{\rho}_{CO2} \overline{w} A_T \qquad (4.10)$$

Some complications occur in the estimation of turbulent flux from the top: the entrainment flux. This flux is difficult to measure because of the intermittent turbulence in the entrainment layer, so it' is usually estimated by parametrization. Lilly et al. proposed a relation connecting this flux to the inversion jump and entrainment rate in a clear convective BL.

The rate of penetration of mixed layer inside the free atmosphere can be written:

$$\overline{w'CO2'}|_{zi} = w_e \Delta CO_2 \qquad (4.11)$$

where $w_e = \frac{\partial h}{\partial t} - \overline{w}_h$

with $\frac{\partial h}{\partial t}$ time rate of change of boundary layer height and w_h subsidence velocity.

A parametrization of the entrainment velocity was suggested by Tennekes (1973):

$$w_e = \frac{A_{f_o} w' \theta_v'}{\Delta \theta_v} \tag{4.12}$$

The subscript 0 in A_{f0} indicate a first order Jump Model (Stull, 1998). The value of this fraction is usually taken at 0.2.

In sea breeze conditions, top height of the control volume should be the CIBL height (see section 2.4). This altitude could be estimated approximately by vertical profile obtained using the mean values of scalars along the legs perpendicular to the coast. This estimation is very rough and does not permit to investigate about the shape of the top of the mixed layer. Moreover, the shape of boundary layer could complicate treatment of subsidence and entrainment terms.

To take into account the increase in mixed layer deep with the distance from the coast (as the case of a CIBL) the top height for the integration could be taken greater than the mixing height (Wratt et al, 2000). If the differences in the horizontal in-flux and out-flux of CO_2 higher up those level are close to zero this choose does not influence the result of the balance. Then it should be stated that the influence of entrainment flux is also null because top is choose in a very stable layer, where turbulence is completely absent.

4.3.1 Flight planning

As discussed in the previous section mass budget methodology requires that the atmospheric conditions during the period of sampling be stationary. To accomplish the goal and in order to have the best performance from the interpolation procedures a standard flight was planned.

Ideal CBLB flight starts during the early afternoon hours and consists in the following steps:

- vertical profile upwind
- several box (rectangular tracks) at different heights inside the boundary layer

- one box at the top of the boundary layer (this could be important both to verify entrainment influence and to indirectly estimate it).
- vertical profile downwind the area of interest

Flight duration should be as short as possible to maintain nearly constant convection, height of boundary layer, wind speed and direction and to avoid any change in the surface properties (emission or absorption rate). Unfortunately the exact planning depends upon the height of BL predicted before the flight. In this work flights were planned without an exact knowledge of BL height because of the lack of instrumentations. Thickness of boundary layer should be measured immediately before the flight by means of lidar or sodar instruments. In the case of coastal area where it's necessary to predict TIBL height it is also possible to use models that requires measurement of temperature difference between sea and inland air, wind and other parameters (Melas et al, 1992, Gryning and Batchavarova, 1990).
The exact estimation will permit to save time for flight since the campaign could be addressed to obtain a better vertical resolution of sampled measurements.

4.3.2 The regression procedures

As described in the section 4.3, in order to estimate total horizontal mean fluxes through the lateral surface of the considered volume the information available at spatial points at which measurements are taken need to be conveyed (estimated) to a different lattice corresponding to the designed surface of the control volume.
In the literature several methodologies were suggested for estimating a function from experimental data (regression). The regression problem could be generally stated as follows: given N points $(\mathbf{x}_i, y_i)$, $\mathbf{x}_i$ being a vector and y_i being measurements at $\mathbf{x}_i$, possibly affected by noise according to the model

$$y_i = f(\mathbf{x}_i) + \varepsilon_i$$

find a function $\hat{f}(\mathbf{x})$ that approximates $f(\mathbf{x})$ in some sense.
For the purposes of the study presented here, parametric and nonparametric methods are considered. In the former an analytical representation of the regression function is known apart of some unknown parameters that are estimated from data, $f(\mathbf{x}, \boldsymbol{\theta})$, with

θ being the vector of unknown parameters to be estimated. Typical solution methods of these problems are least squares and Bayesian methods.

In nonparametric regression no priori assumption is made concerning the analytical shape of the regression function that is instead determined by the method. As a counterpart, the physical problem at hand has to be well described by the analytical function chosen for the parametric case in order to converge to an appropriate solution.

Despite the latter aspect parametric interpolation has a big advantage. Bayesian predictive analysis focuses on the production of predictive distributions for the quantities of interest end as a direct outcome, errors for the estimated parameters can be straightforwardly quantified from McMC iterates, conditioned on the observed data and model assumptions/simplifications (Gilks et al., 1996).

4.3.2.1 Shepard function

Several statistical methodologies exist in the literature concerning non-parametric regression, some of which also extend to the multivariate case. However one of the most used in applied sciences to represent sparse data in the space is surely given by the Shepard function (Shepard, 1968). The regression function is given by:

$$\hat{f}(\mathbf{x}) = \frac{\sum_{i=1}^{N} w(\mathbf{x}-\mathbf{x}_i) f(\mathbf{x}_i)}{\sum_{i=1}^{N} w(\mathbf{x}-\mathbf{x}_i)} \tag{4.13}$$

where the weight function $w(\mathbf{z})$ is given by $w(\mathbf{z}) = |z|^{-\beta}$ with $|\cdot|$ being the usual Euclidean norm and β ranging between 1 and 2; several other weight functions are known in the literature, but they were not consider relevant for the goal of this thesis. It's possible to observe that in the neighbourhood of each data point Shepard function has also an unpleasant side effect, namely the flattening of the interpolatory function due to the fact that by very definition the derivative of the Shepard function is null in the data points. On the other side popularity of the Shepard function comes from its very intuitive nature: actually the regression function in a target point is a weighted average of the values assumed by data all over the volume, with weights decreasing with the distance of the data from the target point. Positivity of the weight function

also makes the estimate very stable, actually forbidding spurious maxima and minima not present in the data.

In the problem at hand it's needed to estimate a regression function of the faces of the box; in addition the high spatial resolution of the data (at least in the horizontal directions) and the flight trajectories not spread around the faces of the box in an erratic (random-like) way makes that the box is far enough from experimental data so that the negative side-effects of the Shepard function close to the data points do not occur (Amato et al, 2007).

For the purpose of this work data are at first rescaled in a local coordinate system having its origin in the projection on the ground of the center of mass of the measurement points and whose axes are chosen to minimize the correlation between components, a numerical grid is then constructed on each face of the box, with varying vertical resolution coherent with the distance between two consecutive legs and fixed horizontal resolution.

The values of CO_2 density and wind speed at the center of each grid cell $\mathbf{x}_{i,j,k}$ can now be determined by the Shepard function: it is identified a suitable neighborhood of that point fixing a radius R (of the order of the chosen horizontal resolution) and selected all data belonging to a sphere of center $\mathbf{x}_{i,j,k}$ and radius R. Then, the weighted average of the observation values within this neighborhood is used as estimate for the considered variable.

4.3.2.2 Bayesian Markov Chain Montecarlo Method

In probability theory, Bayes' theorem relates the conditional and marginal probabilities of two random events. Being X and Y two propositions, Bayes' theorem states that the probability that both "Y and X" are true is equal to the probability that "X and Y" are true. It could be written as:

$$[X/Y,I]\times[Y/I]=[Y/X,I]\times[X/I]$$

If X and Yy are replaced by parameters and data respectively:

$$[parameters/data,I]\times[data,/I]=[data/parameters,I]\times[parameters/I] \quad (4.14)$$

The term $[data/I]$ has the role of a normalizing factor (it not depend from parameters) and could be omitted.

In few world the Bayes' theorem relates the probability that the hypothesis about parameters are true given the data, to the probability that we would have observed the data if the hypothesis are true.

In this work Bayesian method was applied to estimate the parameters of an expression of the type (Ratto et al., 1994):

$$\begin{aligned} \mu\rho &= A_u(x,y)B_u(z/z_0) \\ \nu\rho &= A_\nu(x,y)B_\nu(z/z_0) \end{aligned} \tag{4.15}$$

A_i and B_i are functions that depend on several parameters

$$\begin{aligned} A_i &= a_{1i} + a_{2ix} + a_{3iy} \\ B_i &= b_{1i}\log\left(\frac{z}{z_0}\right) + b_{2i}\frac{z-z_0}{z_0} + b_{3i}\left(\frac{z-z_0}{z_0}\right)^2 \end{aligned} \tag{4.16}$$

where Z_0 is the roughness length.

The equation above is used to interpolate the mean component of the horizontal fluxes, but it's exactly what it's required by the model since it's considered only the mean transport through the lateral surface of the box. In any case the turbulent components are several order of magnitude smaller (Riccio et al, 2007).

Expression adopted for CO_2 interpolation is the linear function:

$$c = c_1 + c_2 x + c_3 y + c_4 z + c_5 z^2 \tag{4.17}$$

Equations above allow the estimation of the mean value of mass and CO_2 flux at any point in the space so that it's possible the extrapolation at any surface. Montecarlo approach is used to estimate the area average surface fluxes. For example, suppose that $\vec{u}\rho$ is a normally distributed variable, i.e.

$$\vec{u}\rho \approx N(\mu,\sigma) \tag{4.18}$$

where μ is the mean value given by (4.16) and σ is the covariance matrix of residuals. If {t} indicates a set of spatial points (the measurement points) and {s} another set (the points at which we interpolate the measurements, i.e. Points corresponding to lattice *H* or *T)*, the joint probability distribution function for a Gaussian variable *x* is:

$$\left[x_{\{t\}}, x_{\{s\}} | \alpha, \beta\right| \approx N\left(\begin{bmatrix}\mu_{\{t\}}(\alpha)\\ \mu_{\{s\}}(\alpha)\end{bmatrix}, \begin{bmatrix}\sum_{\{tt\}}(\beta) & \sum_{\{st\}}(\beta)\\ \sum'_{\{st\}}(\beta) & \sum_{\{ss\}}(\beta)\end{bmatrix}\right)\Bigg] \tag{4.19}$$

So that the conditional distribution of $\left[x_{\{t\}} \mid x_{\{s\}}\right]$ is given by

$$\left[x\{t\} \mid x\{s\}, \alpha, \beta\right] \approx N(\Theta, \Sigma) \tag{4.20}$$

Where $\Theta = \mu\{t\} + \Sigma'\{st\}\Sigma^{-1}\{ss\}(x\{s\} - \mu\{s\})$ and $\Sigma = \Sigma_{\{tt\}} - \Sigma'_{\{st\}}\Sigma^{-1}{}_{\{ss\}}\Sigma_{\{st\}}$.

α and β are the parameters used to model the mean values and the correlations, respectively.

Analogously, the prediction at block areas $\{B\} \equiv (B_1, ...B_k), is$:

$$\left[x_{\{B\}} \mid x_{\{s\}}, \alpha, \beta\right] \approx N\left(\mu_{\{B\}} + \Sigma_{\{Bs\}}\Sigma^{-1}{}_{\{ss\}}\left(x_{\{s\}} - \mu_{\{s\}}\right), \Sigma_{\{BB\}} - \Sigma_{\{Bs\}}\Sigma^{-1}{}_{\{ss\}}\Sigma'_{\{Bs\}}\right) \tag{4.21}$$

$\mu\{B\}$ can be interpreted as the expected values of the spatial average of process x over the blocks $\{B\}$, i.e. the surface of lattice H e T.

Formally, the cell-averaged mean and variances are:

$$\mu_{Bi} = |Bi| - 1\int_{Bi} x ds \tag{4.21}$$

$$\Sigma_{BiBi}' = |Bi|^{-1}|Bi'|^{-1}\int_{Bi}\int_{Bi'}\Sigma_{ss'} ds ds' \tag{4.22}$$

$$\Sigma_{Biy} = |B_i|^{-1}\int_{Bi}\Sigma_{sy} ds \tag{4.23}$$

$|B_i|$ denoting the area of the i[th] cell. As outlined in Gelfand et al., (2001), it' possible to evaluate via Monte Carlo integration, it can be selected L uniformly distributed points over cell $Bi, \{s_l, : l = 1, ..., L\}$ and $S_l \in B_i$, and replace (4.21) by

$$\mu B_i \approx \frac{1}{L}\sum_{l=1}^{L} x_{(s,s_l)} \tag{4.24}$$

Cell variances can be similarly estimated:

$$\Sigma_{BiBi'} \approx \frac{1}{L^2}\sum_{l=1}^{L}\sum_{m=1}^{L}\Sigma_{s_l s'_m} \tag{4.25}$$

$$\Sigma_{Biy} \approx \frac{1}{L}\sum_{l=1}^{L}\Sigma_{s_l y} \tag{4.26}$$

Where $s_l \in B_i$ and $s'_m \in B_{i'}$. Those approximations can be made arbitrarily accurate, by letting L be sufficiently large.

This procedure was adopted to evaluate the area- averaged CO_2 concentration at the top surface, and the CO_2 fluxes through the lateral face of the virtual volume.

Chapter 5: Experimental flight campaign over Piana del Sele

5.1 The flight campaign

In the following sections the application of the mass balance method to an agricultural site located on the western coast of Italy, close to Salerno city (details are given in section 5.1.1) will be described.

This area is suitable for the investigated method since local sea breeze during the daytime is present. The local wind intensifies (or prevail on) the existing synoptic wind with its horizontal component orthogonal to the coast. This implies that a large concentration difference between the downwind and upwind sides of the flight domain is present due to the fact that the air coming from the sea is poor in CO_2. This condition is desirable in applying mass balance method. Moreover the constant influx from the marine environment assures a spatially homogeneous distribution on windward side that also is a suitable condition for the applicability of the method.

The pattern flown during the experiment was dedicated to the documentation of 3-D wind field and CO_2 concentration inside the box owing to compute the advection terms in the chemical specie budget. A careful data analysis is performed in order to identify the TIBL height (section 5.1.2).

5.1.1 Experimental setup and data observation.

Piana del Sele is located in southern Italy, close to Salerno city. It's a typical Mediterranean landscape where the land use is mainly arable cropped to highly fertilized field crops and vegetables (corn, tomato, artichoke, potato and fodders) with numerous plastic tunnels. A narrow belt of pine forest is located in the West side representing about 15% of the entire surface. Between the forest and the mixed area there is an urban area bordered by a road.

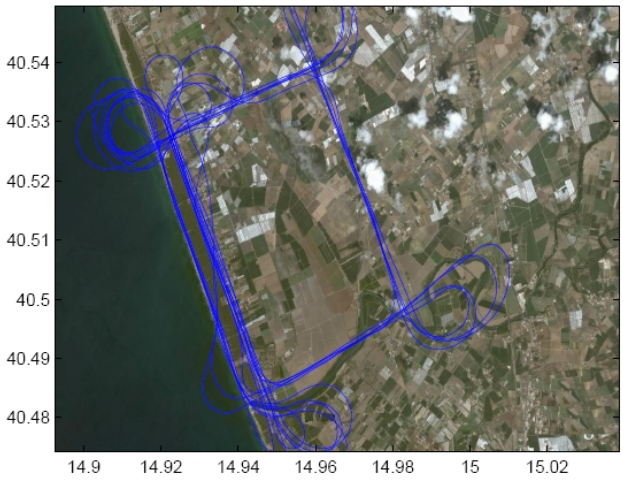

Figure 13: Flight trajectories flown on 1st of August 2006 over the Piana del Sele Landscale

The campaign was performed on the 1st of August 2006 during the afternoon (about 14:30 local time) and the flight pattern was planned to design two different boxes, one bordering the forested area, and the other the mixed cropland (Figure 13). The sampling was done in calm wind synoptic condition (1-2 m/s). This implies that the measured wind during the flight was only due to the local scale advection (sea breeze).

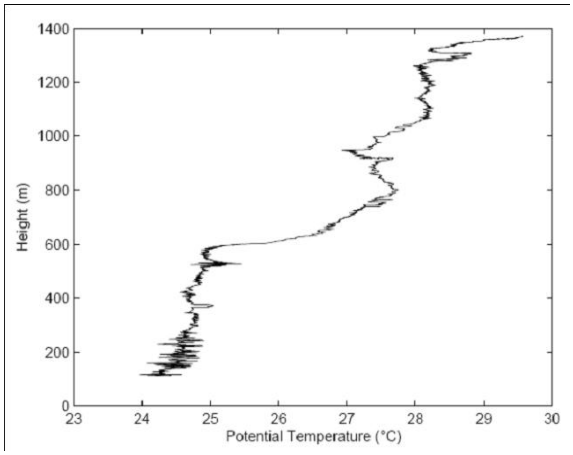

Figure 14: Potential temperature profile measured by aircraft at 10:30 UTC on the 1st August 2006.

Figure 15 shows both wind speed and direction measured by the meteorological ground station in "Borgo Cioffi", site located at the east boundary of the selected area. Right panel describes the typical variation in wind direction during the few days before the campaign. Sea breeze front typically arrives at about 9:30 local time,

marked by a wind direction shift, while in the afternoon sea breeze gradually becomes weaker, and it is replaced by the prevailing offshore wind. Data in Figure 15 also shows that, typically, wind speed maintains constant values during the afternoon hours with similar magnitudes between the 11:30 and 15:30 UTC.

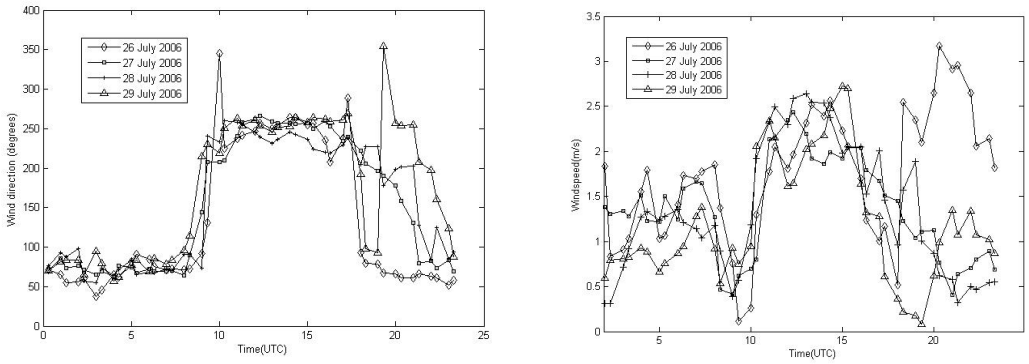

Figure 15: Wind speed and direction measured by sonic anemometer at the "Borgo Cioffi" ground station.

Time of flight falls within that time interval. This could assure stationary conditions required by mass balance technique. The mission started at 12:29 UTC so as for the whole period of flight steady state conditions were expected. Also, incoming solar radiation was sufficient to maintain strong turbulent activity by convection.

A marked Potential temperature jump was detected at 10:30 during a vertical profile (Figure 14). Potential Temperature profile shows a well developed Boundary Layer.

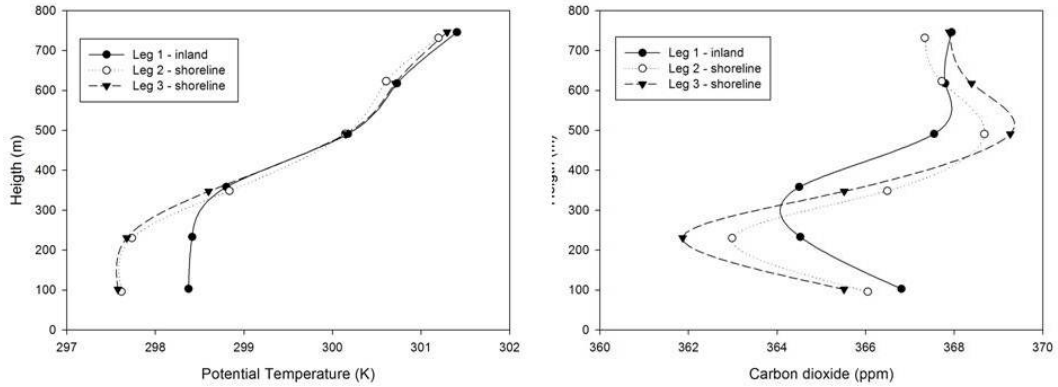

Figure 16: Vertical profiles of CO_2 (on the right) and Potential Temperature (on the left) averaged along the legs parallel to the coast. Measurements are referred to the flight mission performed at 12:30 UTC.

The structure of the lower troposphere changed considerably with the onset of sea breeze and became increasingly complex, with an increasing number of layers until the evening (Talbot et al., 2007). At the time of flight sea breeze was at an advanced stage and a typical stratification occurred.

From the scalars observation (Figure 16) it's possible to distinguish three different layers: the sea breeze layer extending until 400 m, while a residual boundary layer until 550 m and the free atmosphere above. Sensible Heat Fluxes show a BL height at 550 m as well, since the minimum value is located there (see definition gave by Deardorf – section 2.2.2). This is observable only considering the leg flown inland. Sensible heat fluxes near the coast are close to zero because of the vicinity to the sea. This altitude corresponds to about the boundary layer height detected at 10:30 UTC (Figure 14).

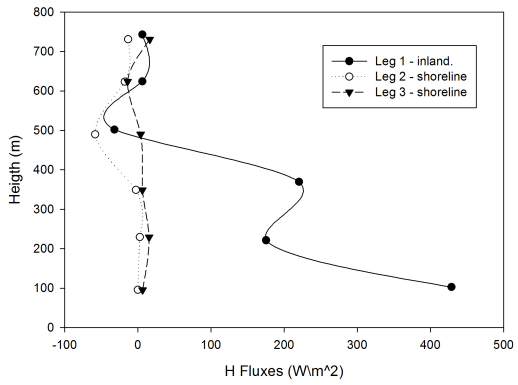

Figure 17: Latent heat fluxes calculated along the legs parallel to the coast. Legs are numbered as function of distance to the coast (leg 1 is the closest to the coast).

5.1.2 Determination of TIBL height

Thermal Internal Boundary Layer structure was investigated through a careful observation of the acquired data. Potential temperature measured along the legs close to the coast shows a jump between 250 and 350m height (right panel of Figure 16). Different behaviour is shown by the profile performed inland, where Potential temperature is nearly constant with height until 350 meters.

CO_2 concentrations profiles present the same vertical shape of the potential temperature (left panel of Figure 16). Lower CO_2 values are starting at 200 m signing

the effect of the gravity current (air coming from the sea). Water vapour mixing ratio increases from the ground to the top of the TIBL (not showed), also indicating a mixing due to the shearing of continental air masses and gravity current in the vicinity of sea breeze front.

To better understand the evolution of the Thermal Internal Boundary Layer the Turbulent Kinetic Energy (TKE) over the entire area was calculated. The TKE calculation was performed along the legs orthogonal to the coast with steps of 100 m at each altitude covered by aircraft. These values have been finally interpolated (showed in Figure 18). Due to strong stability and low production of mechanical turbulence, turbulent kinetic energy in the maritime boundary layer is low so that the top of turbulent layer is only 350 m. Over the land TKE is higher than over the shoreline because of buoyant production. Convective boundary layer is very shallow close to the shoreline and increases gradually up to 350 m at about 4.5 Km downwind the shoreline.

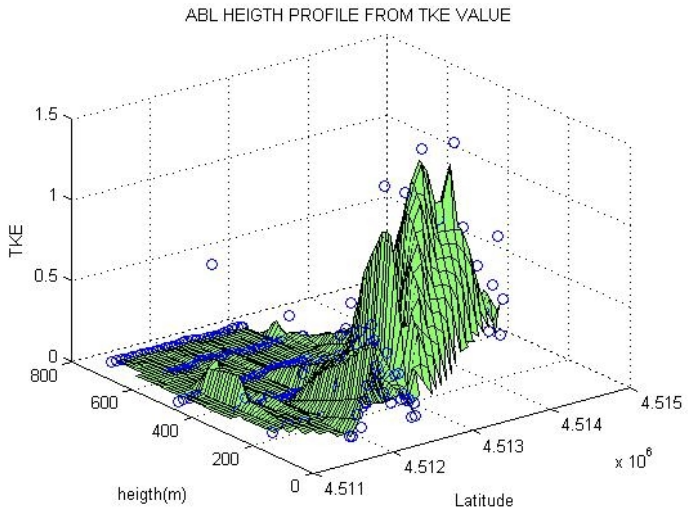

Figure 18: Turbulent kinetic Energy calculated along the leg south-west (perpendicular to the coast). Blue circles represent values calculated by aircraft. Green surface represents the interpolated values.

Weisman model (Weisman, 1976) was used to compute the growth of the TIBL downwind the shoreline. The model has been tested by several scientists (Petersen, 1999), and has been proved that it provides the best estimation when compared against field observations. The Weisman equation makes the assumption of constant

overwater temperature lapse rate, uniform overland wind profile, constant surface heat flux, and zero heat flux at the top of the TIBL. Equation has the following form:

$$h_b = \sqrt{\frac{2H_{0,\infty}x}{\alpha C_p \rho U_L}} \qquad (5.1)$$

Where h_b is the height of thermal internal boundary layer (TIBL) at distance x (m); $H_{0,\infty}$ is the surface heat flux far inland (W/m2); α is the overwater potential temperature vertical lapse rate ; and U_L the average wind speed within the TIBL (m/s).

Input required by model has been calculated using the available data and are showed in Table 1.

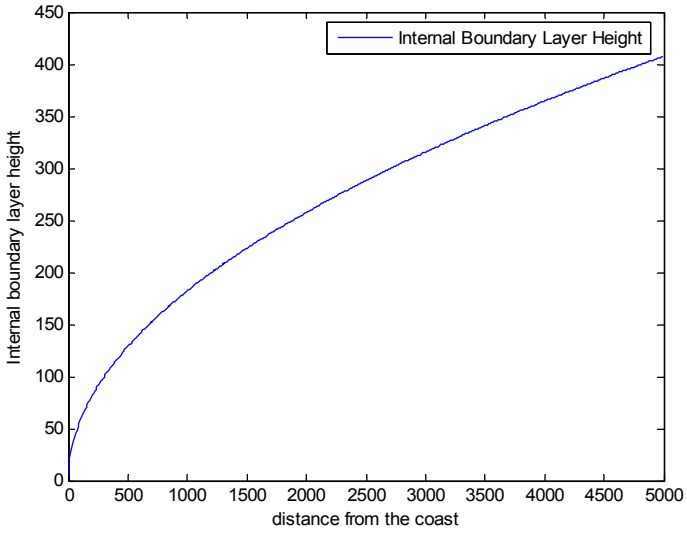

Figure 19: TIBL height modelled by the Weisman function

H_0 (W/m2)	α (K/m)	Cp	ρ (Kg/m3)	U_L(m/s)
450	0.0040	1005	1.16	6.30

Table 1: ***Input data of Weisman model calculated from available data***

Even though the simplicity of the model, there is agreement between the theory and experimental results. This was probably because the assumptions, on which the model is based, seem to be fulfilled, as also suggested by data observations. Choose

of sampling time assure stationary condition so that parameters alpha and Ho can be considered constant. Also wind intensity is constant during the whole flight.

5.2 Mass budget application : results and discussion

In this experiment averaged CO_2 fluxes have been estimated via mass balance for two different areas: the belt of forest close to the sea and the composite cropland inland. Both Shepard and MCMC methods have been used to estimate mean CO_2 fluxes over the lateral face of the air column.

As discussed in the previous section atmosphere at the time of flight was stratified and two inversions were detected: one at the altitude of about 350 m (corresponding to the CIBL height) and another at 600 (corresponding to a residual BL).

Observing the difference in CO_2 concentration measurements between the leg inland and that close to the coast (Figure 20) it can be noted an inversion at 300 m where the values changes from negative to positive. It was expected that an inversion will be also detected in the signs of fluxes estimated by mass balance method, if analyzed as function of the top height of the virtual volume (H_{top}). In spite of considerations above, mass balance approach was applied changing the height H_{top} and results were compared.

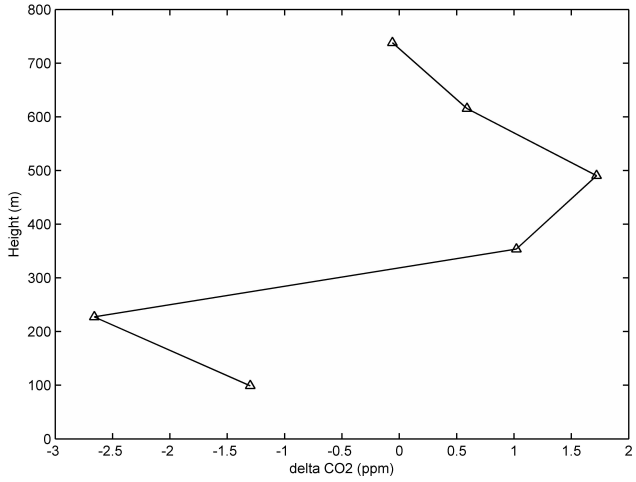

Figure 20: CO_2 concentration differences between the legs located on shoreline and that inland.

The first step in applying Shepard method is the definition of a virtual box on which to construct the interpolation grid and integrate flux values. The virtual box should be as close as possible to the experimental points to minimize the error of predicting CO_2 density, air density and wind on the box.

Therefore, the first test done owing to verify the Shepard method is applying successful is that the lateral planes of the volume well fit the flight trajectories at the different heights. In this case a good agreement was found so as it is expected that interpolation procedure provides representative values of wind and scalars over the selected domain.

Interpolation grid is chosen so that the centres of each cell are located in the middle of the trajectories flown by aircraft.

The horizontal resolution in the evaluation of lateral fluxes ranges from a minimum of 6.4 m, corresponding to 100 cells on each of the horizontal level, to a maximum of 51 m. Table 1 reports in the estimated CO_2 emissions for the cropland area as a function of resolution and height of the virtual box. Box heights has been chosen so as to fall close to 300 and 600 m height in order to compare the results and their variability both as function of height H_{top} and horizontal resolution of the interpolation grid. Choosing the height of 300 m the results are small emissions. It can be noticed that the estimated area average surface fluxes above the area are very variable as function of H_{top} .

Top Height (H_{top})	***Horizontal resolution***			
(m)	***51***	***22.5***	***11.3***	***6.4***
300	8.41	10.45	10.38	10.47
310	7.14	9.06	9.13	9.20
320	5.87	7.67	7.89	7.94
330	4.60	6.28	6.64	6.67
340	3.33	4.89	5.39	5.41
350	2.06	3.50	4.15	4.14
550	-14.48	-12.77	-12.48	-12.44
560	-15.01	-13.20	-13.04	-12.98
570	-15.43	-13.53	-13.35	-13.31
580	-15.86	-13.86	-13.66	-13.64
590	-16.29	-14.19	-13.97	-13.98
600	-16.71	-14.52	-14.28	-14.31

Table 2: Estimated CO_2 emissions in µmol/m2/s for the Eboli cropland area as function of resolution and top height.

If the altitude H_{top} is set to around 600 m height the estimated CO_2 flux is an absorption of about -13.44 micromol/m2 /s (mean value considering the higher resolution of the interpolation grid). This value seems to be a more reliable estimate when considering the land use of the area mainly consisting in croplands. Moreover the sampling period is referred to a summer day in which is expected an intense photosynthetic activity.

Starting from 550 m height, the balance through the air volume remains constant giving about the same values at increasing H_{top} altitudes. The variability within 100 m is about +- 2 μmol/m2/s.

Changing the horizontal resolution does not imply a great variability in the results if the cell size is smaller then 22.5 m. Instead a large size of the cell (51 m) doesn't give a good spatial representation of wind and scalars over the face of the control volume, resulting in a larger estimate of surface fluxes.

The proposed methodology was also applied to data measured surrounding the forest area to yield an estimate of the pine forest assimilation rate. Being a very narrow area, it was expected the results to be very sensible to the choice of box vertices and boundary layer height. Indeed, in every configuration the results confirm a significant absorption (about -20 μmol/m2/s) from this surface, for a top height comprised in the range 200-300 meters. Note that at this location the presence of the sea led to a shallow CIBL as well as a stable layer above it. Stratification found inland it's not present in this area.

Bayesian McMC approach was also applied to estimate CO_2 flux over Piana del Sele. In the following results will be exposed.

In order to apply the Bayes' theorem, *a-priori* distribution for parameters has to be selected in equations (4.15). It was chosen a conjugate normal distribution for all parameters, assuming data normally distributed. Then, joint posterior distribution is normal too.

To check the feasibility of Bayesian approach it's necessary to check that equations (4.15) remove non-stationarities. As can be note residuals are effectively normal distributed (Figure 21).

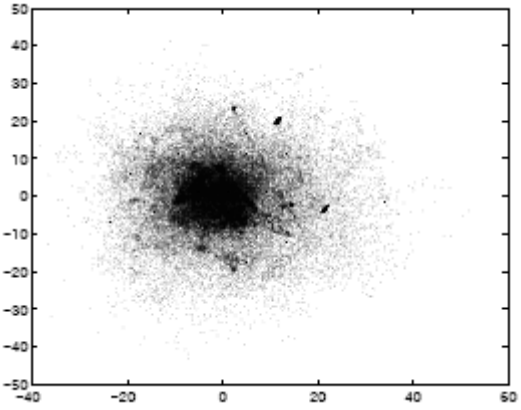

Figure 21: residuals for the x and y direction.

The mean values of priors were estimated by preliminary data exploration and all parameters were assumed to be *a-priori* uncorrelated. An inverse-Wishart distribution was used to sample from the posterior distribution of the covariance matrix of parameters. Errors were computed by batching, to account for the correlation in the Markov chain (Roberts, 1996). 5000 iterations were used to gain confidence in the estimated errors.

In Figure 22 and Figure 23 are shown the histograms representing the relative frequency of CO_2 fluxes estimations derived from MCMC iterates.

The CO_2 estimation over the forested area gives absorption with a median value equal to -17 μmol/m2s (Figure 22). This result is comparable with that from the Shepard method application. It should also been noted that the results for the forest show a greater variability, which depends on the fact that parameters in equation (4.15) are more weakly identified. Presumably, the proximity to the sea makes the identification more problematic, though this aspect needs a deeper understanding.

Concerning the mixed area the implementation was done for two different values of the height H_{top}, 300 m and 550 m. Figure 23 shows the estimated CO_2 flux from the surface, as a function of McMC iterates in the different imposed boundary conditions.

As can be noted, over the mixed area also has been estimated an absorption (median value equal to -3.16 µmol/m^2/s), if the height H_{top} is assumed to be at 550 m height. Instead, considering an estimated value H_{top} equal to 350 m the results is a little emission (median values equal to 5.22 µmol/m^2/s) as also observed using Shepard

interpolation. Interpolation by Shepard approach tends to gives greater absolute values of CO_2 emissions.

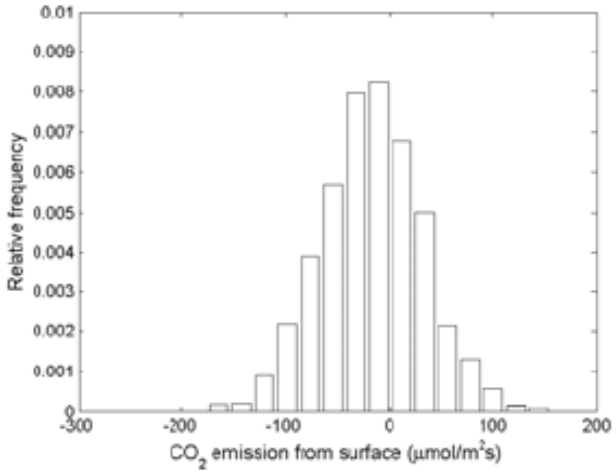

Figure 22 : Hystogram of estimated CO_2 surface fluxes (forest) as function of MCMC iterates (H_{top}=350).

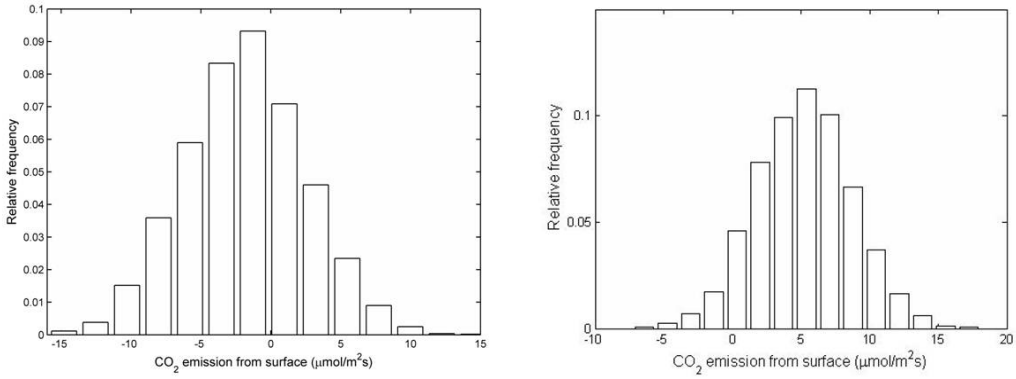

Figure 23: Estimated CO_2 surface fluxes (mixed area) as function of MCMC iterates. On the left : H_{top}=600; On the right: H_{top}=350.

In order to assess the validity of mass balance approach CO_2 surface flux was calculated by Eddy covariance method starting from data sampled during the campaign.

Because of the heterogeneity of the area to obtain a term to compare the method it would be required the installation of a ground station network which is impractical and unaffordable.

Another possibility is the quantification of turbulent fluxes of the surface by performing a series of low level flight with enough repetitions to average out the

variability. As already discussed because of steady state assumption required by model, flight have to be as short as possible so as it is not possible to apply Eddy covariance (AEC) at the same time of flight, unless another aircraft is used in the same campaign.

In this work footprint analysis was done in order to find a proper leg on which AEC could be calculated giving a CO_2 flux that is representative of the whole area. The flux footprint is the contribution per unit emission from each element of a surface area source to the vertical scalar flux measured at a certain height above the surface. In this analysis, the footprint estimations are carried out using the simple analytical footprint model proposed by *Hsieh (2000)*. In Figure 24 is represented the CO_2 flux calculated along the leg parallel to the coast (inland) end the relative footprint plotted on the map. The leg chosen was flown at a mean altitude of 100 m. As could be noted footprint surface comprise the most part of the mixed area. Eddy covariance was calculated on the whole leg (length is about 4.5 Km) resulting in a CO_2 flux of -13.46 μmol/m2s. The values are in agreement with results from mass balance approach, if the height H_{top} is equal or greater than 550 m.

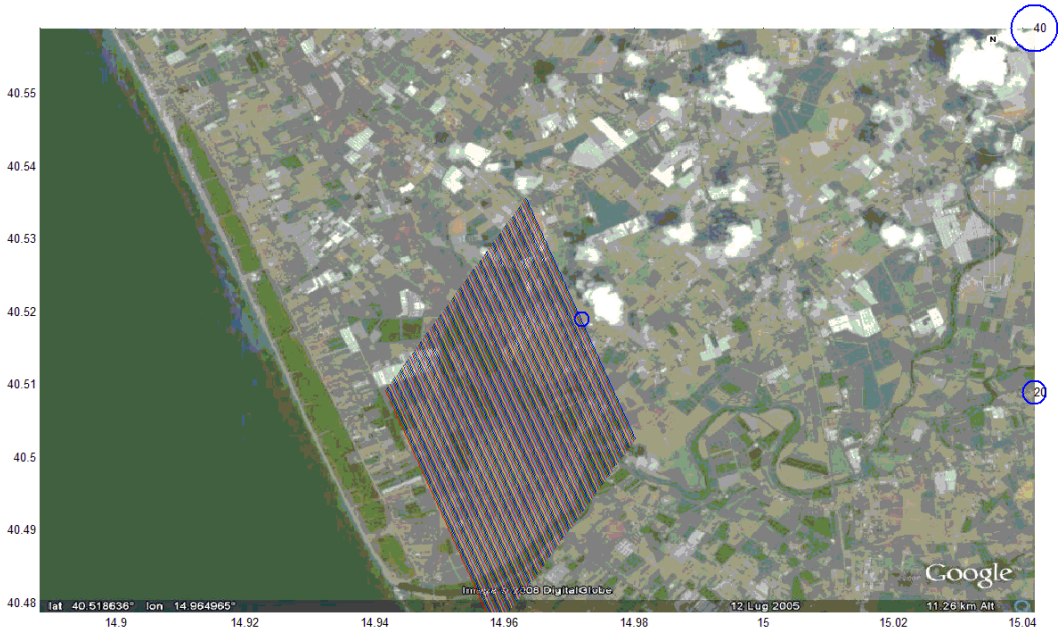

Figure 24: Representation of the footprint relative to a leg that has flown at 100 m altitude. Blue circle represents CO_2 flux (absorption) calculated along the leg inland.

Chapter 6: Experimental campaigns in Sardinia Island

In this chapter are examined measurements performed at several site at high anthropogenic activity located in Sardinia island. Region of Sardinia was chosen being isolated from any surrounding stress in terms of CO_2 emission because the area is completely bordered by the sea. Moreover as for the National Forest Inventory it's is considered the most forested area of Italy. As a counterpart it is indicated by the National Emissions Inventory as the second region per CO_2 emission (per unit of GDP).

Mass balance method was applied to estimate the relevance in terms of CO_2 emission of the main industrial sites over the whole region and to identify the major source of emission. Another question rising is the investigation about the capability of agricultural site of the area to absorb the emission from anthropogenic activities.

As exposed in Chapter 2 the development of the Thermal Internal Boundary Layer over coastal areas could be the reason of the entrapment of pollutant in the lower layers of the atmosphere leading to negative consequences for human health. Vertical profiles of various meteorological parameters were also analysed to investigate vertical and horizontal structure of coastal boundary layer and the role of sea breeze in affecting distribution of main pollutants in the low atmosphere. Finally, mass balance methodology is applied, comparing the results from the interpolation procedures explained in Chapter 4.

Sardinia is a peculiar case: although its main characteristic is the high vegetated surface density, the most part of industrial activities are located close to the coast. Concentration of CO_2 in these areas could be very high though the absorption from surrounding area might contribute to diminish the average concentration over the whole island. Campaigns were devoted to monitoring of the main industrial poles and cities in the south of the island.

Cagliari is the most inhabited city of the region hosting about 33% of the entire population of the region. The most important industrial activities in this part of the

island are represented by those related to the oil refineries: the main poles are located in the areas of Machiareddu (Cagliari), Sarroch (Cagliari), and Portoscuso.

6.1 Experimental Setup

Missions were performed in tree days (4, 6 and 7 June 2007) and each experiment started at about 14:00 local time. Portoscuso's industries were monitored on the 4th of June. During the second day (6th of June 2007) the aircraft flew above both the areas of Sarroch and Machiareddu. Campaign preformed on June the 7th was devoted to sampling the city of Cagliari while Sarroch area was also monitored again.

6.1.1 Portoscuso Mission

The campaign performed on the 4th of June 2007 was addressed to monitoring the city of Portoscuso. Rectangular patterns were flown around the city (see figure 1) at four different altitudes (250, 400, 550, 750 m a.g.l.), circumnavigating the main source of emissions. The industrial pole of Portoscuso (primarily consisting in refinery industries) and a landfill (located in the south west side of the flight pattern in Figure 13) are among the most important sources of trace gases in the area.

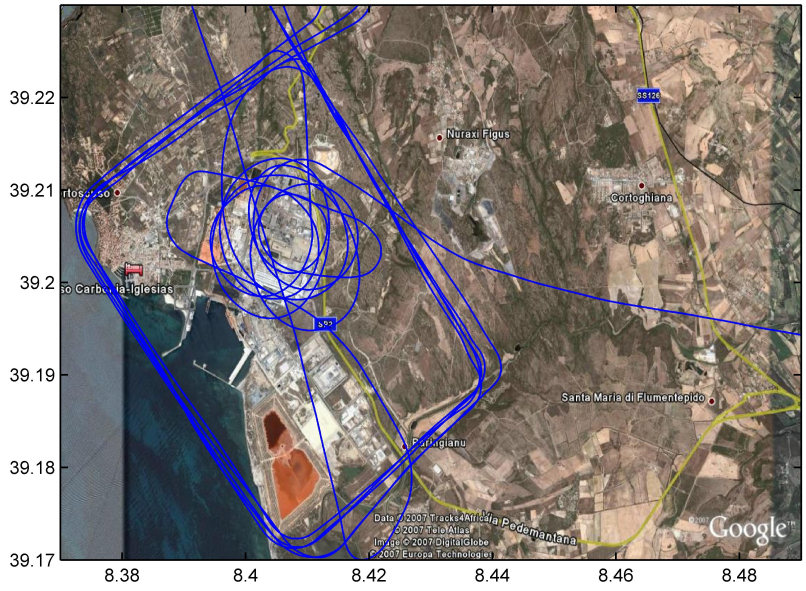

Figure 25- Flight pattern flown over Portoscuso on 4 June 2007

Two vertical sounding profiles were performed by using the airborne platform in the centre of the studied area. These profiles were performed before and after (Figure 25) the measurement flight, owing to better define a priori assumption of meteorological steady state conditions.

During the mission the prevailing wind was mistral. The wind direction was quite constant showing variation between 300 and 330 degrees, while the wind intensity measured along the cross legs of the rectangular pattern, showed a variation from 5.5 m/s, on sud-west side of the box, to 7 m/s on north-east side (Figure 26). The reasons for the lower wind magnitude measured offshore compared with inland, could be due to the influence of the sea breeze coming from south-west. It was also observed a decrease in turbulence on the south-west side of the flight domain.

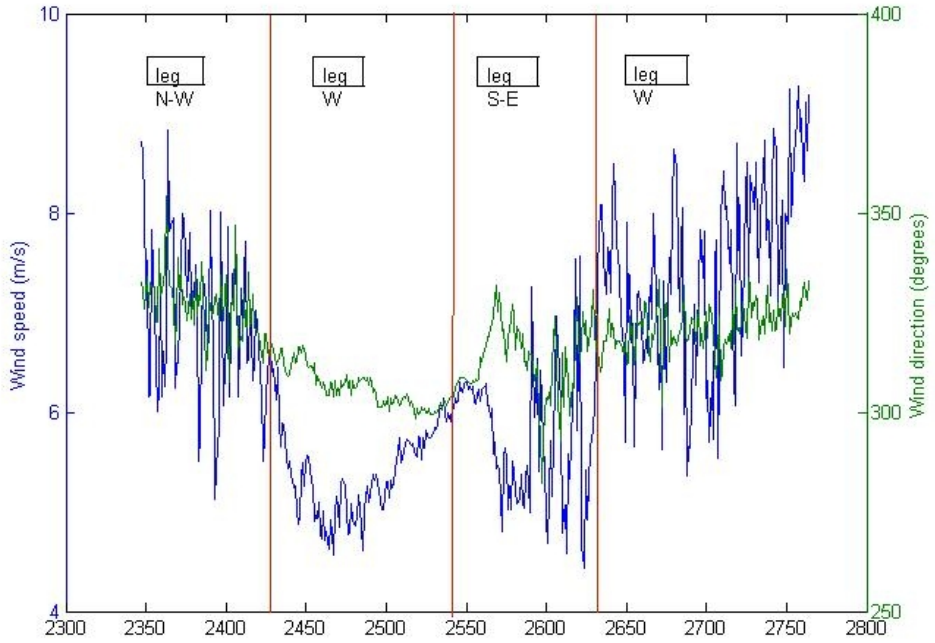

Figure 26: Wind intensity (blue line) and direction (green line) at 245 m height.

In Figure 27 and Figure 28 water vapour and potential temperature are plotted versus height. These data were collected during the vertical profiles performed before (on the left side) and after (on the right side) the flight mission.

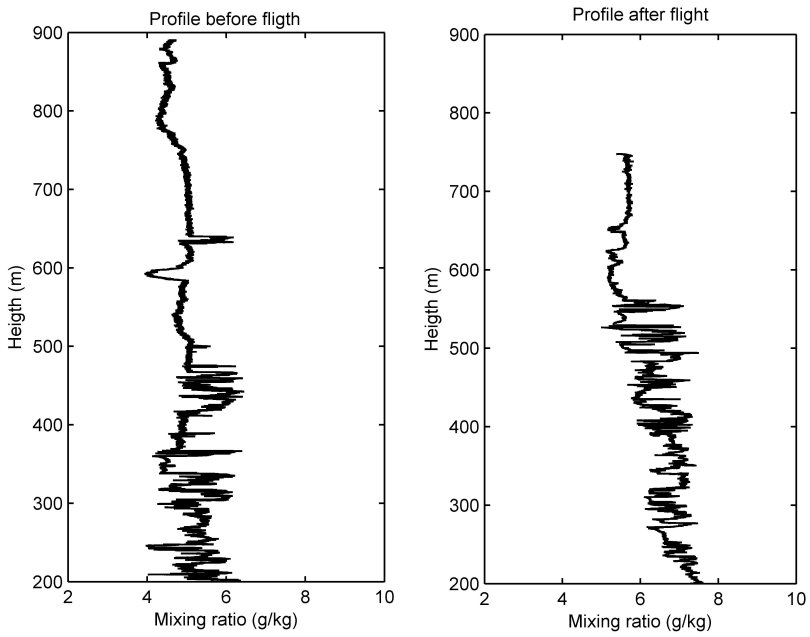

Figure 27: Mixing ratio vertical profiles before (left panel) and after (right panel) flight.

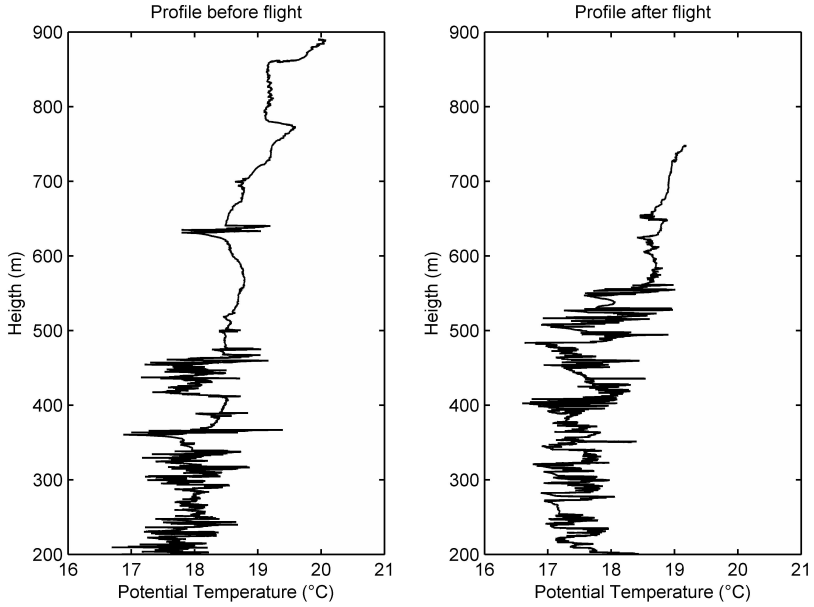

Figure 28: Potential Temperature of vertical profile flown before (right panel) and after (left panel) the flight.

The top of the Boundary layer was not identifiable by a clear inversion. As it can be noted there isn't any evident change neither in potential temperature nor mixing ratio

can be found. A sudden decrease in turbulence at the height of 500/550 m both in the mixing ratio and potential temperature measured during vertical profiles. Potential temperature values have only a slight increase at that height.

Profiles data indicate that steady state conditions were probably maintained during the time of the flight. Inversion height only increased 50 m during the whole duration of flight (90 minutes). This corresponds to a small value of $\frac{\partial z}{\partial t}$ equal, approximately, to 0.85 cm/s (in absence of subsidence).

More humid air was measured on west and north sides of the box because of the advection of marine air from north-west (Figure 30). A Carbon dioxide plume has been detected over the downwind side, on the southern leg (Figure 29).

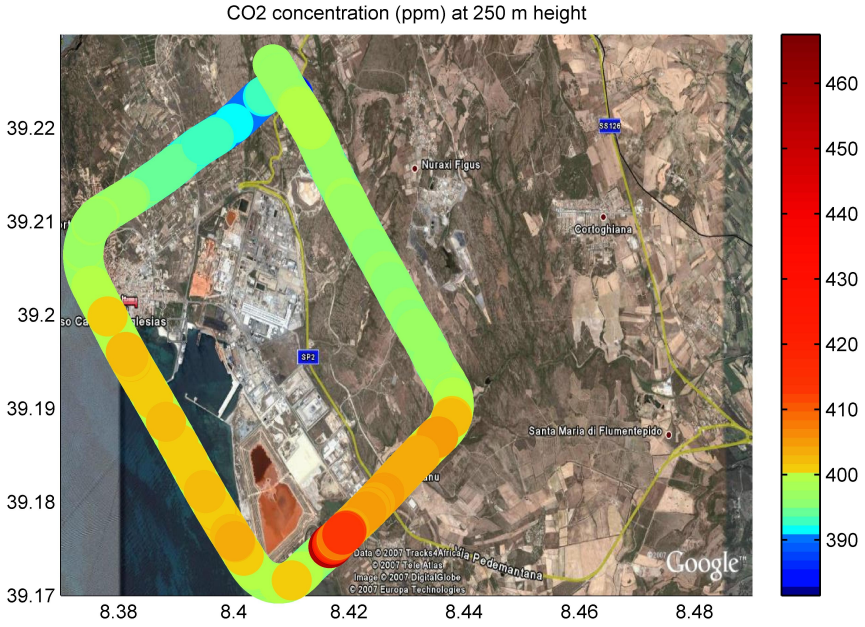

Figure 29: scatter of CO_2 concentrations measured over Portoscuso at 250 m height

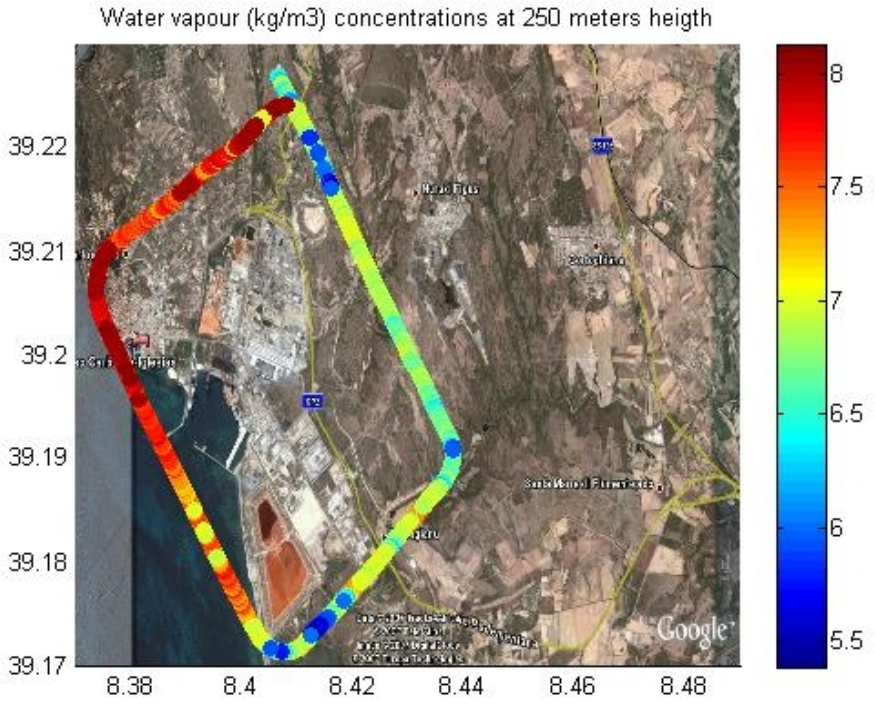

Figure 30: scatter of water vapour concentrations measured over Portoscuso at 250 m height

Moreover it was observed an enhancement in CO_2 concentrations as function of altitude (Figure 31). It is supposed that the gas was strongly spread vertically because of the convergence of different sea breeze systems on the area. Also the strong turbulent activities could contribute to this effect. The hypothesis was confirmed by the high positive value of vertical velocity measured during the mission (about 0.2 m/s).

CO_2 plume were found until the height of 550 m. Above this height the plume vanished and CO_2 concentration notably decreased, sign of the presence of a "lid" trapping the pollutant in the lower layers. The height of the lid coincides with the inversion noted by the observation of potential temperature profiles.

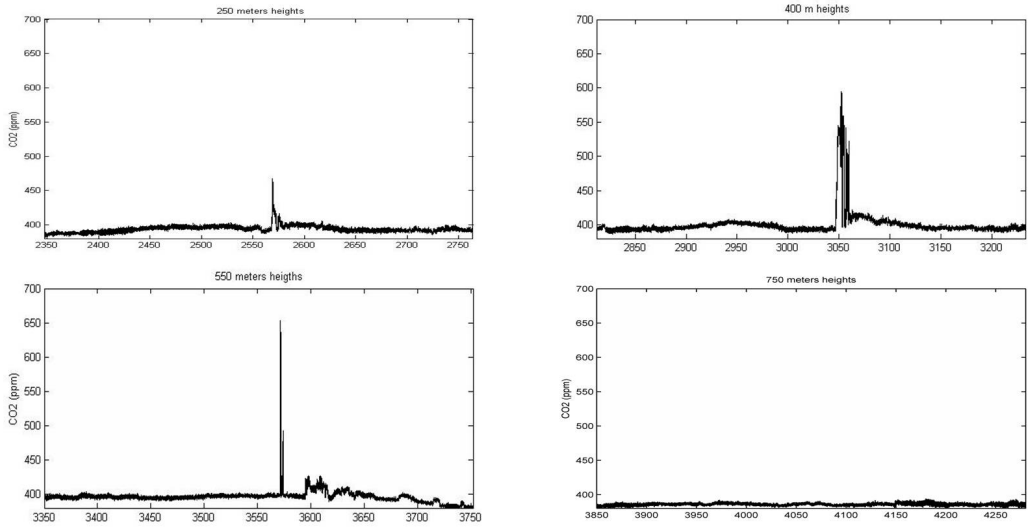

Figure 31：CO_2 concentration over the pattern flown by aircraft at different heights

Figure 32 shows the vertical behaviour of the scalars and wind at each side of the box (legs are named according with the position which respect to the box). Data prove the presence of an inversion at about 550 m with a decrement in water vapour, and an increment in Potential temperature and CO_2 concentration above that height. The greater values in CO_2 concentration correspond to a similar behaviour in wind speed. Sea breeze is stronger at that height.

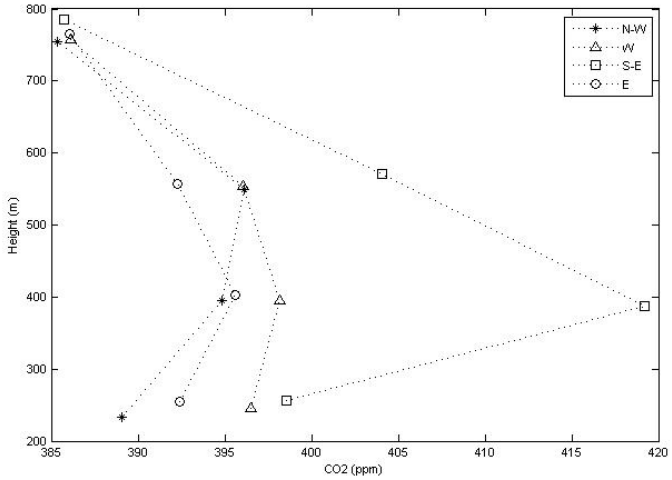

Figure 32: CO_2 values averaged over the 4 legs as a function of altitude.

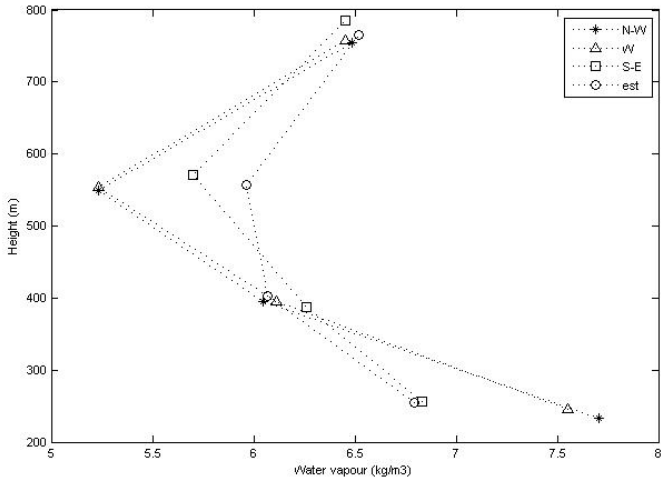

Figure 33: H2O values averaged over the 4 legs as a function of altitude.

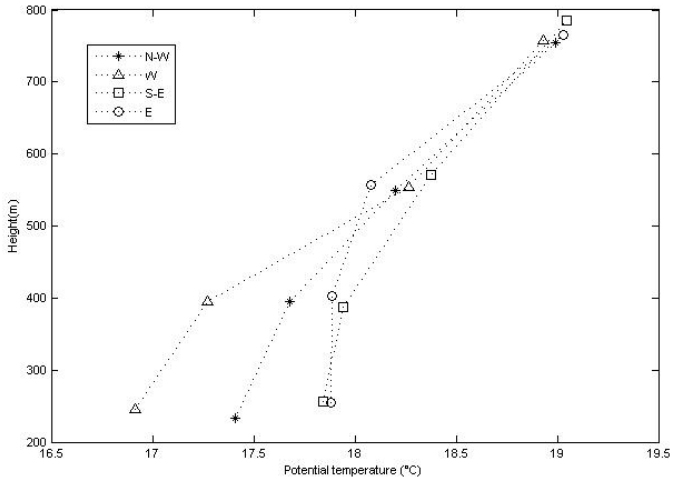

Figure 34: Potential temperature values averaged over the 4 legs as a function of altitude.

6.1.2 Machiareddu and Sarroch mission

During the flight mission performed on the 6th of June 2007, the aircraft flew a rectangular pattern over the main industrial districts close to the city of Cagliari: Machiareddu and Sarroch. Flight patterns were designed on the basis of the standard flight described in 4.3.1. Boxes above Machiareddu were flown at the heights of 100, 150, 200, 350 and 500 meters.

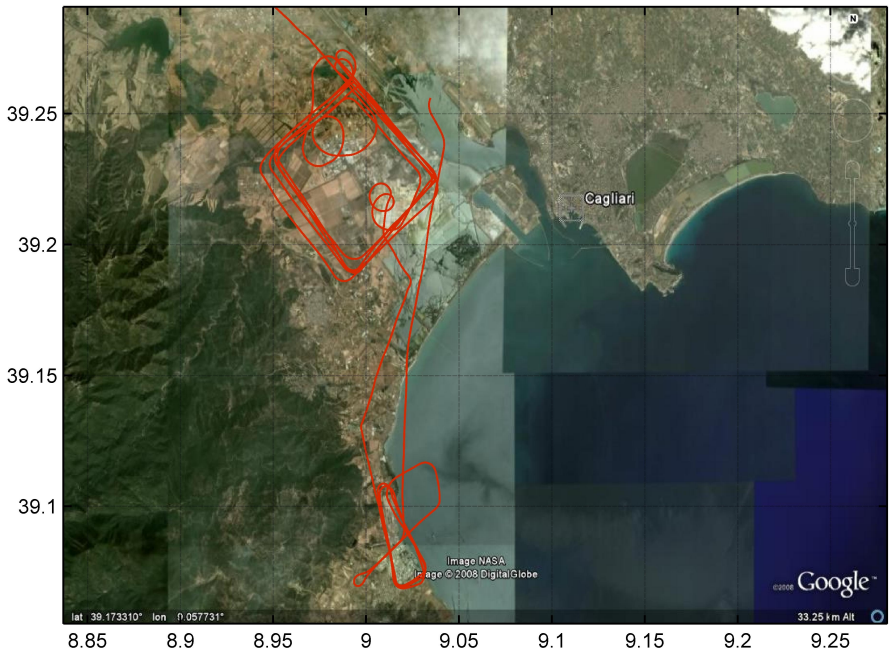

Figure 35: Flight pattern flown by aircraft on 6 June 2007 over Machiareddu and Saras

Sarroch industrial site is a very small area and located in a position where convergence of different sea breeze system occurs. As consequence questions arose about the feasibility of the mass balance method application because of the difficulty in founding adapt experimental condition (wind orthogonal to the coast). It was decided in any case to fly over the area with the main goal to monitor the CO_2 concentrations.

Figure 35 shows flight patterns over Machiareddu. It could be noted that the location where vertical profiles were flown differs from that chosen for the flight over Portoscuso. In this case, in fact, it was decided to perform a profile upwind (at about 3 Km from the shoreline) and another downwind (inland) so as to verify the variation of TIBL height as function of distance to the coast. Missions were merely exploratory, in the sense that it was not used a standard flight plan, so as to probe the capability of the mass balance method using different experimental conditions.

We did not expect a big variation in TIBL height as a function of the distance from the coast because the leg closest (and parallel) to the shoreline was located 3 Km

inland where TIBL is already well developed. This was confirmed by the vertical profiles of potential temperature (Figure 36) showing only a small difference between the downwind and upwind sides that is probably a sum of both the effects due to the spatial (as function of the distance to the coast) and temporal (the upwind profile was performed at the end of the mission) variation of Thermal Internal Boundary Layer Height. Mean BL height was estimated at about 250 m.

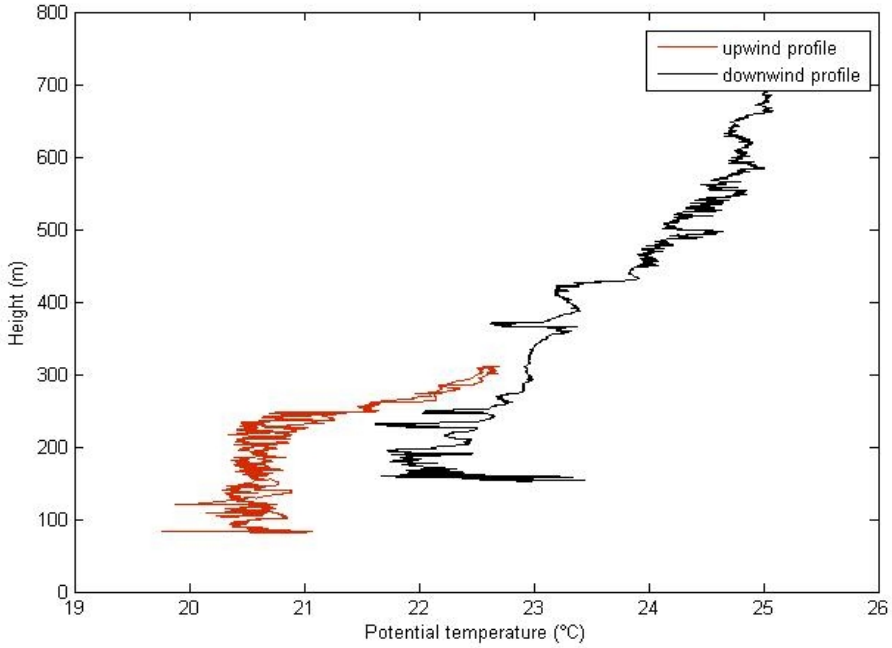

Figure 36: Potential temperatures profiles over Machiareddu area.

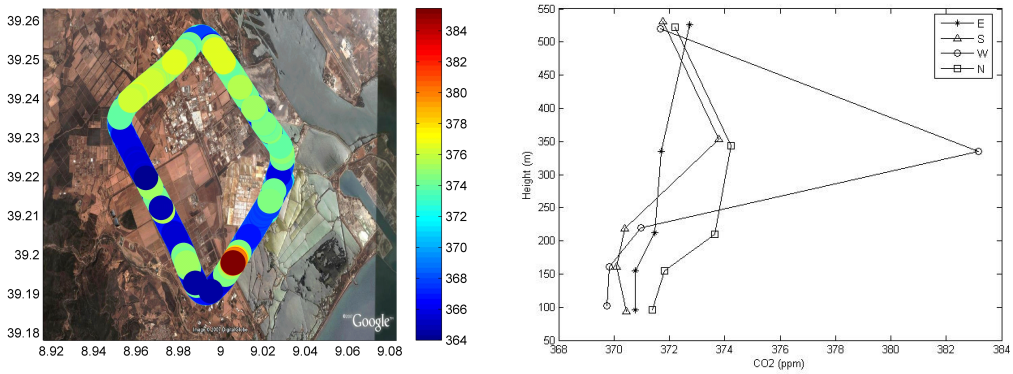

Figure 37: On the right panel: scatter of CO_2 concentrations sampled over Machiareddu area at 100 m height ; On the left panel means of CO_2 concentration calculated over les at the altitudes flown by aircraft.

Low CO_2 concentration has been detected at 100 m height that highlight small emission sources in the area (Figure 37). The monitored surface comprises only an industrial area on the north east side that represents about 30% of the entire domain. Large part of the remaining terrain is covered by cropland that contributes to diminish the mean concentration above the domain studied, by sequestering CO_2. Moreover, there is a quite constant shape of the CO_2 concentrations in the vertical direction indicating again a small gas source on the ground (Figure 37).

Mean wind blowing from south-east takes polluted air on the downwind side (detected on the North West corner of the box in Figure 37-right panel).

Wind measurements reveal the presence of an East component of the mean wind that adds to sea breeze flow. The result is a mean wind breeze not exactly perpendicular to the coast. This is evident from mean values of wind measurements calculated along the leg. Observing the vertical profiles in Figure 38 it can be noted that at the uppermost altitude, where sea breeze has no effect, both wind speed and wind direction have a marked shift.

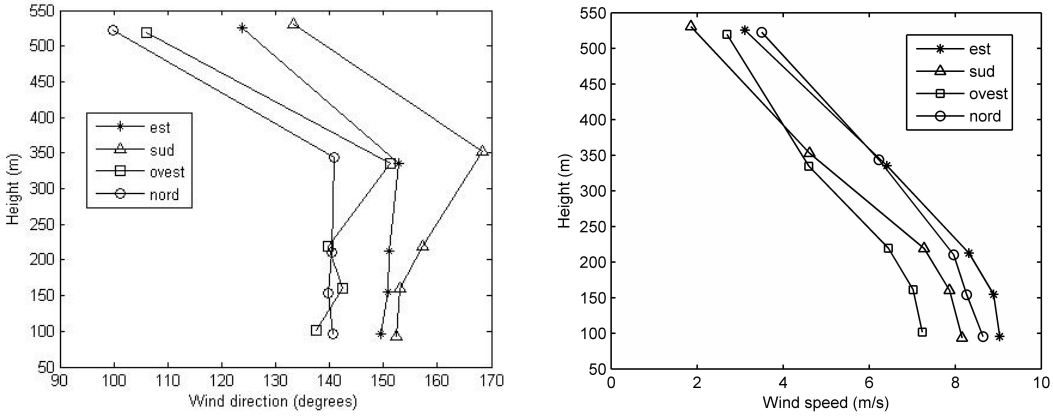

Figure 38: Wind speed (on the right panel) and direction (on the left panel) averaged over legs as a function of altitude.

Observing wind profiles (Figure 38) it could be detected a further inversion at which the sea breeze influence seems to notably decrease. This corresponds to a height of about 350 m.

The explorative mission over Sarroch confirmed that the location of industrial area makes difficult the application of the mass budget approach. Prevailing wind is from south-west as a result of the convergence of two sea breeze system. The vectorial composition yields a mean wind blowing orthogonal to the smaller sides of the box

(about 1 km). Then, measurements taken upwind and downwind the area are insufficient and not representative.

In Figure 39 is shown the CO_2 concentrations measured during the whole flight over Sarroch. The highest concentrations are observed along the eastern side of the box (Figure 35), corresponding to the first leg flown by the aircraft.

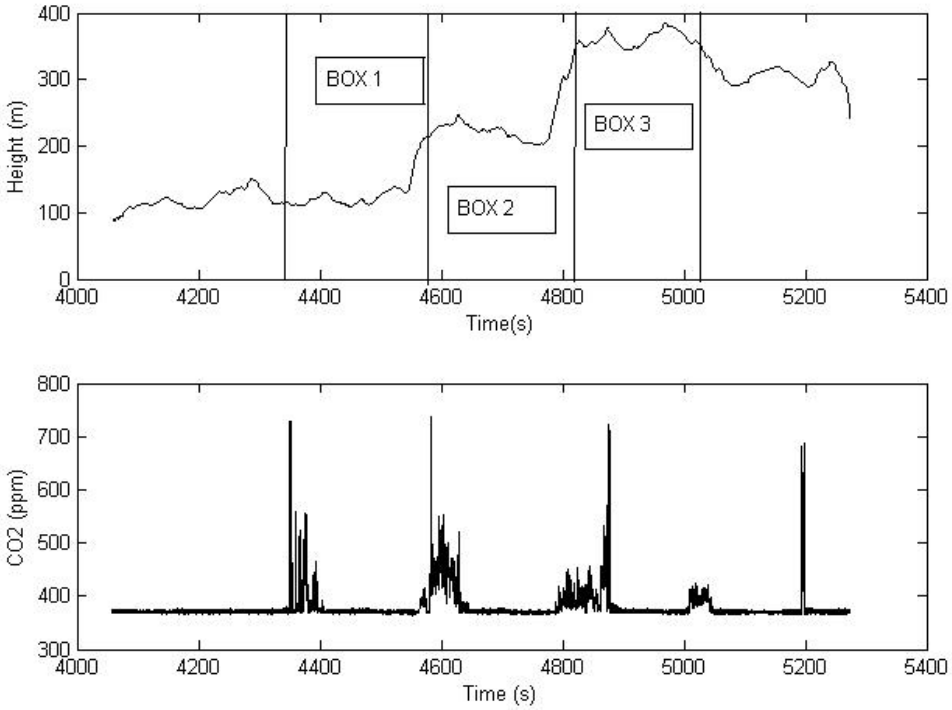

Figure 39: Altitude (upper panel) and CO_2 concentration (bottom panel)

6.1.3 Mission on Cagliari city

Last experiment was carried out covering the city of Cagliari and subsequently the industrial pole of Sarroch. Mission started at 14:06 local time so that the mission over Sarroch started at about 15:30. A rectangular shape flight was flown above both areas of interest (see Figure 40).

Table 3 indicates the altitudes covered by aircraft during the two missions.

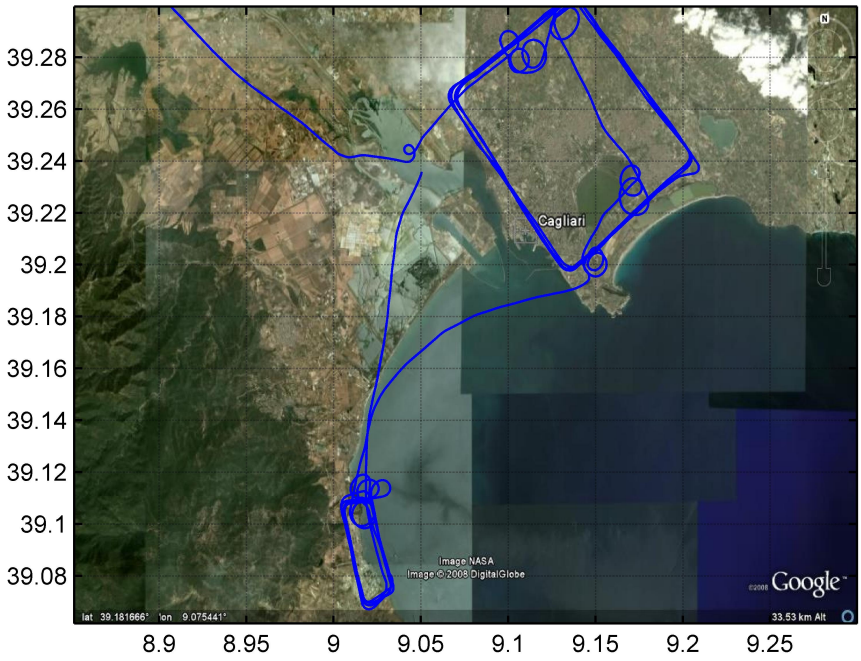

Figure 40: Flight trajectory flown by aircraft on 7 June 2007

Site	***Height (m)***			
Cagliari city	150	230	350	530
Sarroch	150	250	370	520

Table 3- Altitudes flown by aircraft over the sites: Cagliari and Sarroch

First profile, flown downwind the city of Cagliari, evidences a slight potential temperature inversion at about 300 m height (Figure 41). At the end of the mission a vertical profile was performed close to the sea, on the upwind side. In this case the inversion was observed at about 350 m height. It could be also noticed that at about 100 m height the turbulence vanishes: this height probably corresponds to the TIBL height above the shoreline, although it was not possible to distinguish a clear inversion, especially when observing mixing ratio measurements (not shown).

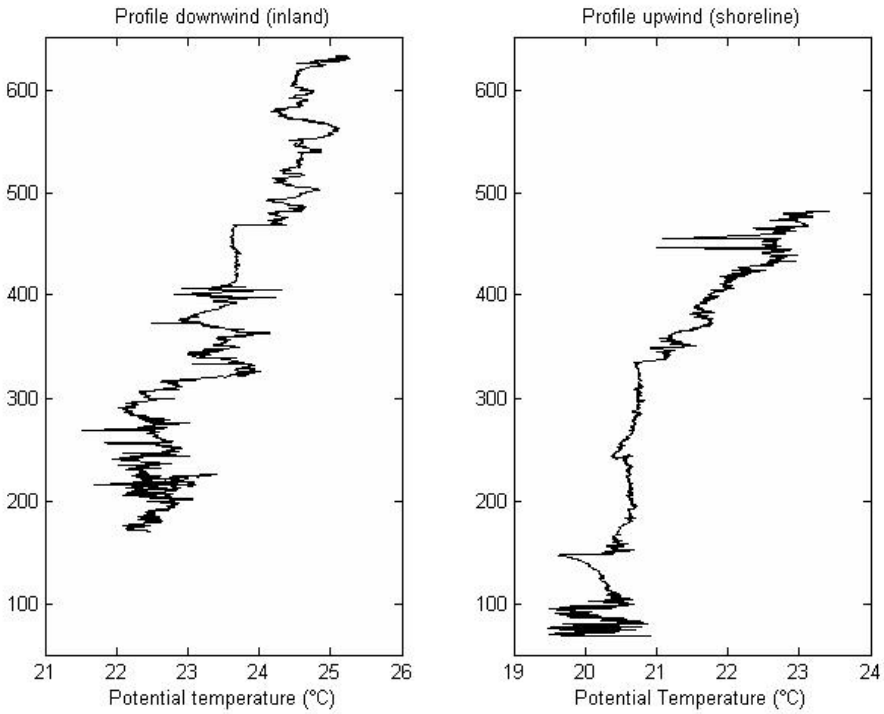

Figure 41: Potential temperature profiles flown downwind and upwind the city of Cagliari

Mean values of Potential temperature along the legs do not show a clear inversion as well (Figure 43). Instead atmosphere seems to be stable observing that data. An appreciable inversion could be seen in CO_2 and wind data (Figure 42 and Figure 44). Though it is expected a positive CO_2 flux (absorption) in the area, the enhancing of CO_2 as function of height (Figure 42) seems to indicate the presence of a source of absorption on the surface. This could also be an effect of advection from the sea since the layer at which the CO_2 concentrations are diminishing (until 350 m) coincides with the portion of the atmosphere where sea breeze has effect (indicated by wind speed values).

Wind direction is prevalently onshore (south /south-east) though a west component is important on the west side of the flight domain.

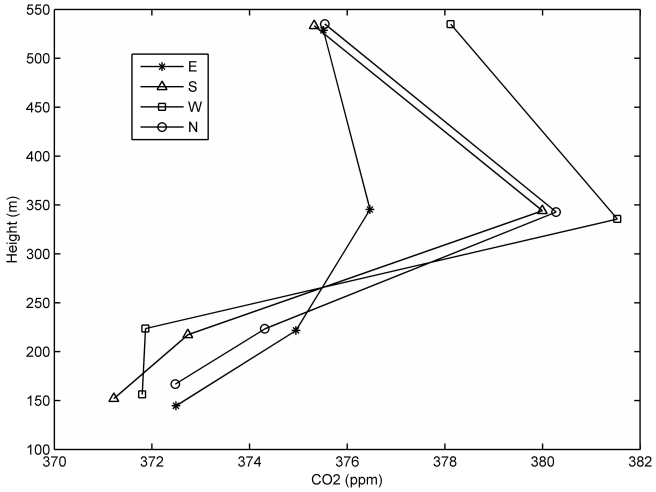

Figure 42: Means of CO2 concentration over legs flown by aircraft as function of altitude

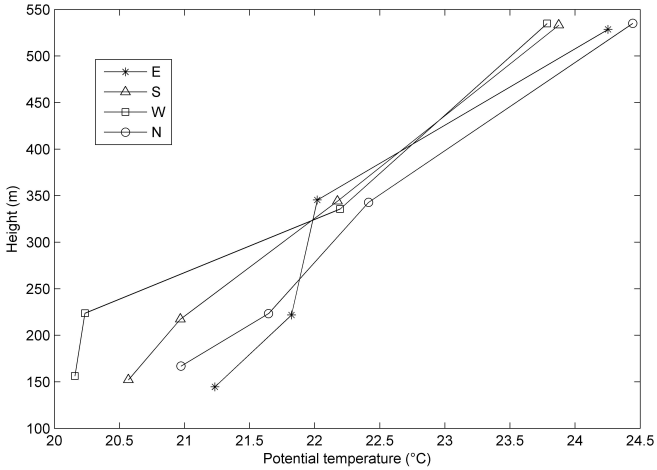

Figure 43: Means of potential temperature over legs flown by aircraft as function of altitude

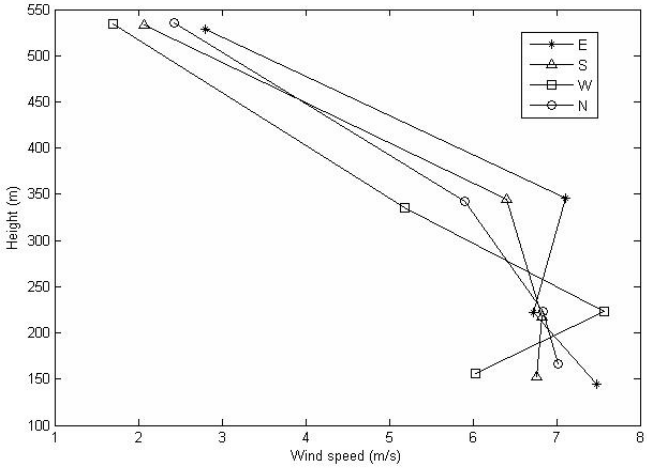

Figure 44: Means of Wind speed over legs flown by aircraft as function of altitude.

The monitoring of Sarroch area shown to have any utility for the determination of area averaged CO_2 flux over the selected domain. Both wind speed and direction are very variable along the flight pattern since its mean value is the results of a main component from west due to the synoptic wind and another one from south due to a dominant sea breeze system (Figure 45).

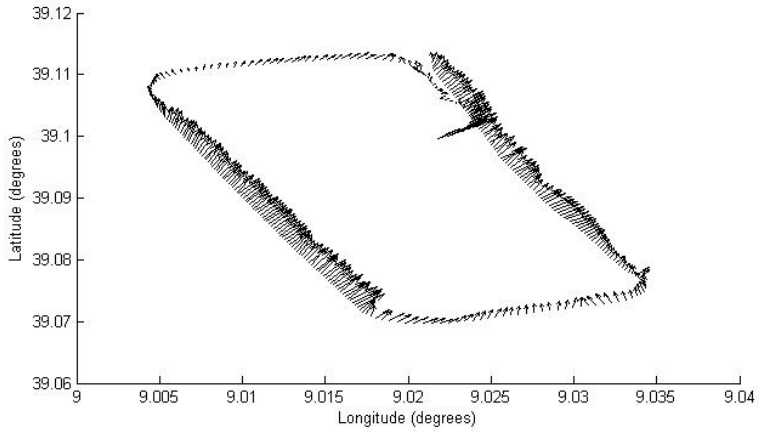

Figure 45: Wind vectors of measurements sampled at 150 m height over Sarroch area.

Moreover it was not possible to define a boundary layer height since the aircraft was forced to fly too close to the sea to avoid chimneys, finding a stable atmosphere.

A tentative to perform mass balance over the area yields a negative balance (absorption) as result, for any combination of the boundary conditions (H_{top} height, vertices and definition of the interpolation grid). Results are not considered reliable since the area is entirely occupied by refineries where combustion is the main process.

6.2 Results and discussion

Mass balance approach was used to estimate emissions/absorption in the monitored areas. Both Shepard interpolation function and Bayesian method have been used to interpolate data over the lateral face of the selected air column, in each one of the experiments.

To investigate about the magnitude of the impact on the total CO_2 flux estimation due to urban and industrial areas as well as the extent of main sinks present within

the flight domain, soil use macro-areas has been extracted from CORINE land use map.

In Table 4 are summarized estimated H_{top} height and the surface of the investigated areas, for each experiment.

Site	*Estimated H_{top}*	*Surface*
Portoscuso	500	18.26 km^2
Machiareddu	250	28.26 km^2
Cagliari city	350	72.70 km^2

Table 4: estimated H_{top} and surfaces of the domain for each experiment

6.2.1 Portoscuso experiment : result and discussion

Provincial Emission Inventory arranged by the "Province of Cagliari " in 2002 estimated that the area of Portoscuso accounts for 28.8 % to the total CO2 emission of the province, while only 3% is produced in Cagliari city. The estimation related to Cagliari city comprises emissions becoming from both the industrial area of Machiareddu and the downtown of Cagliari.

The main emissions sources in those areas are due to the combustion from industrial plants devoted to the metalwork and electricity production.

A rough estimation of annual CO_2 emission above Portoscuso was extracted from the National Emission Inventory (INES) for the years 2005 and 2006. In Table 5 are shown the main industries comprise within the flight domain and the relative CO_2 emissions. The inventory takes into account plants emitting a quantity of CO_2 greater than 100000000 kg/y.

Name	*Unit*	*CO_2 emissions 2005*	*CO_2 emissions 2006*
Alcoa Trasformazioni S.r.l	Mg/y	249234	247052
EURALLUMINA S.P.A.	Mg/y	901109	880087
UB Sulcis - ITE Portoscuso	Mg/y	714189	668013
UB Sulcis - ITE Sulcis	Mg/y	1468186	1537017

Table 5: Annual CO_2 emissions from the main industries in the area of Portoscuso (INES 2005-2006).

As pointed out, a CO_2 plume was detected on downwind side of the flight domain (Figure 29). It's supposed that the major contribution of that plume became from the landfill site located on the south-west corner of the sampled area.

CO_2 area average fluxes estimated by Shepard method are shown in Figure 46. Results show large sources of emission that was also confirmed by INES data and by aircraft measurements. For horizontal resolution smaller than 11 m, integration of CO_2 fluxes over the control volume tends to give the same CO_2 emission values.

Estimated mixed layer height is about 550 m. As can be observed, starting from this altitude, the estimated CO_2 surface fluxes are stable around the mean value of 155.57 µmol/m2/s (considering horizontal resolution equal or smaller than 11 m).

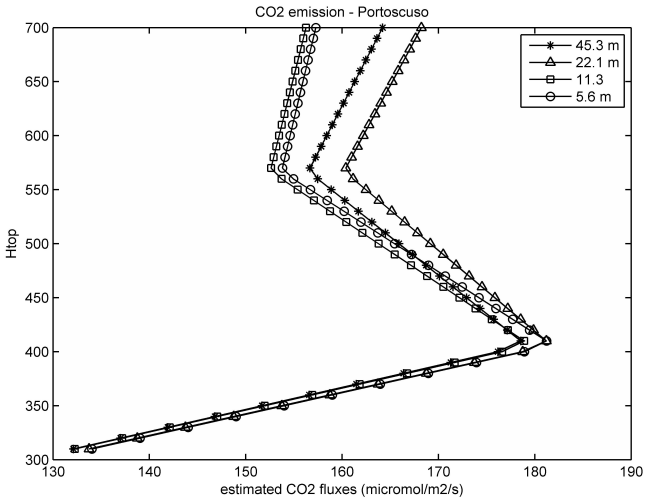

Figure 46: CO_2 emissions in µmol/m2/s over the area of Portoscuso estimated by Shepard method interpolation plotted as function of H_{top}. Legend indicates the horizontal resolution of the interpolation grid.

Because of the detection of a high CO_2 plume localized on the leeward side of the area a question raises about the influence of those huge concentrations on the total balance of CO_2 fluxes over the air volume. The hypothetical effect of this point source could be an overestimation of CO_2 emissions or a different behaviour of the regression procedures in representing the scalar fields. It was also supposed that the contribution of the plume should be referred only to the origin of the source (landfill).

In order to investigate how the plumes could affect the total balance and consequently the estimation of surface emission it has tried to apply the method in two different cases:

- *Case 1*: CO_2 plumes were cut off from CO_2 time series:
- *Case 2*: CO_2 time series as measured by sensor.

Figure 47 represents the CO_2 measurement in the two different cases.

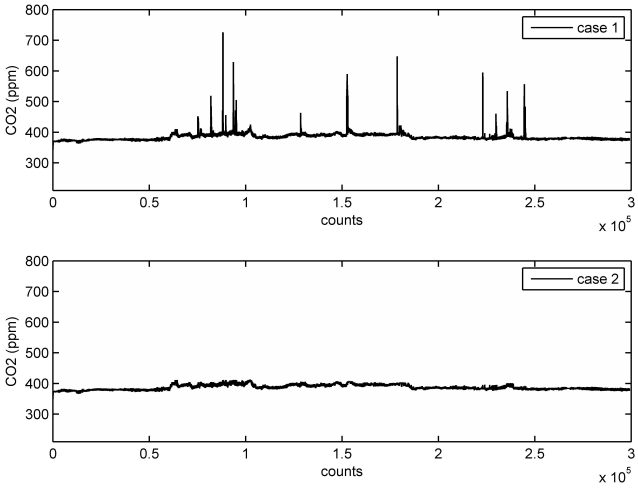

Figure 47: Upper panel: CO_2 concentration measured during mission over Portoscuso; bottom panel: CO_2 time series without plumes.

Considering a height H_{top} equal to 550 m, results from Bayesian method estimated as function of McMC iterates produce a median values of 192.4 µmol/m2/s in the case 1 and 379.7 µmol/m2/s in the case 2. Instead, considering an horizontal resolution of 5.6 m (and H_{top}=550), interpolation by Shepard function gives a CO_2 estimate of 93.83 µmol/m2/s in the case 1 and 155.39 µmol/m2/s in the case 2. In general, Shepard interpolation gives smaller CO_2 emission values than Bayesian Method. Moreover, the estimated contribution due to CO_2 plumes (in few words is smaller using Shepard function than applying Bayesian approach. This difference is of the order of 30/50 µmol/m2/s using Shepard and about 200/250 µmol/m2/s using Bayesian method. This effect is probably due to the differences between the two methods.

In the Shepard method the weight function used to interpolate data is based on the distance of the grid point from the data. Therefore the method is fully local and takes account of possible peaks only in those cells that are close to them. As consequence,

the CO_2 peaks are accounted for over a small surface of the lateral downwind plane. Moreover, the one of the main properties of the method is an averaging effect on the measurements that tends to smooth the horizontal CO_2 fluxes over the lateral surface of the box.

In Figure 48 are shown the results from Bayesian approach plotted versus MCMC iterates. As can be noted, using the CO_2 time series as measured by sensor the MCMC iterates produce a bigger variability in the resulting CO_2 emissions (Figure 48). Parameters of the function (4.15) are not well identified probably because the methodology is global and estimates the CO_2 fluxes through parameters that are global, that are the same all over each blocks. Therefore peaks in the measurements risk to bias the estimate all over the block. It can say that the methodology is less robust to the hypothesis of the underlying model.

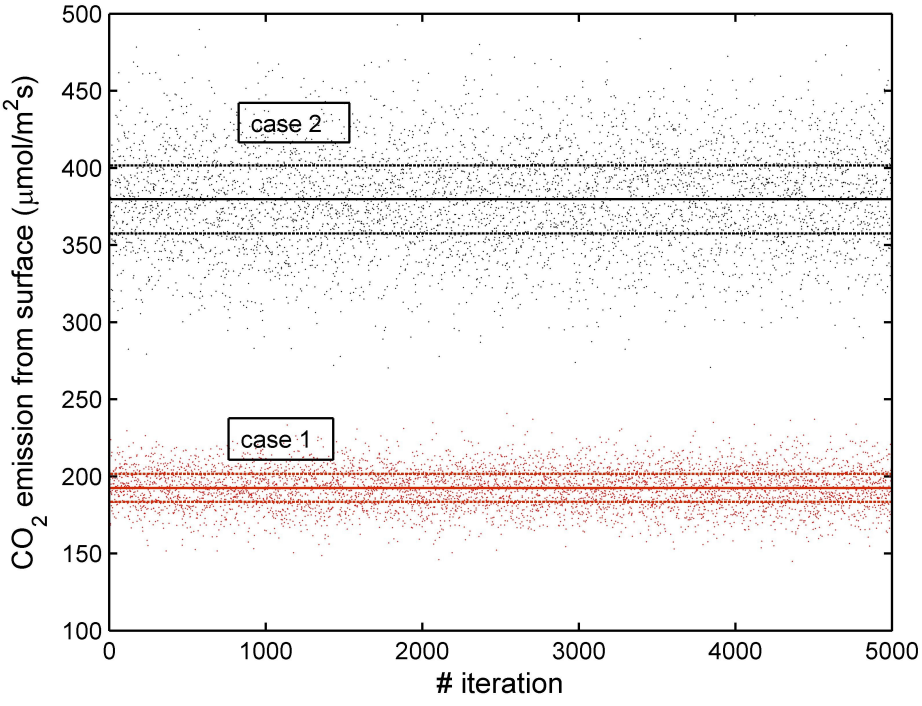

Figure 48: CO_2 fluxes estimations as function of MCMC iterates for the two considered case. Fill line represents the median value. Thin line is median value from the iterations and dotted lines represent the range. Portoscuso experiment.

CO_2 estimations were compared with CO_2 emission inventories derived by INES database.

Available emissions data represents a cumulative sum of the CO_2 emissions from the main Industries in the area of Portoscuso and are referred to the whole year (years 2005 and 2006 were taken into account in order to observe the annual variability of the emissions since data were not available for the year 2007). Assuming a constant CO_2 emission during the year, an estimation of the CO_2 flux per second was calculated. In Table 6 are summarized the comparison between the CO_2 surface fluxes estimations derived in the present work (results are represented in Kg/s and for an H_{top} values equal to 550 m).

Case 1		***Case 2***		***INES***	
Bayesian method	***Shepard method***	***Bayesian method***	***Shepard method***	***2005***	***2006***
154.58	75.38	305.06	124.84	105.67	105.66

Table 6: Comparison between CO_2 surface flux estimation over the area of Portoscuso (top height = 550 m)

The results seem to be quite in agreement with estimation extracted from INES inventory. Anyway the CO_2 fluxes calculated by Bayesian method, particularly in case 1 are not considered a valid estimation because of the reasons exposed above.

CO_2 emissions estimated by mass balance method are referred to a time of the day at which we expected an intense activity of the industrial plants, while values extrapolated by INES inventory has been equally smear over the whole year to derive a flux per second. Then it's obvious that the estimation gives greater values of CO_2 surface flux above the area. However, the reader has to take into account that the comparison performed has its limitations due to the approximations adopted and its use for the validation purpose have to be carefully analysed.

In igure 49 are shown macro-areas, extracted from CORINE land use, inside the flight domain of Portoscuso. It's highlighted that positive contribution to the total emission over the area is large. Only 35% of the total surface (Figure 50) is covered by agricultural landscape. Moreover the Industrial pole includes industry typologies at high emission potential.

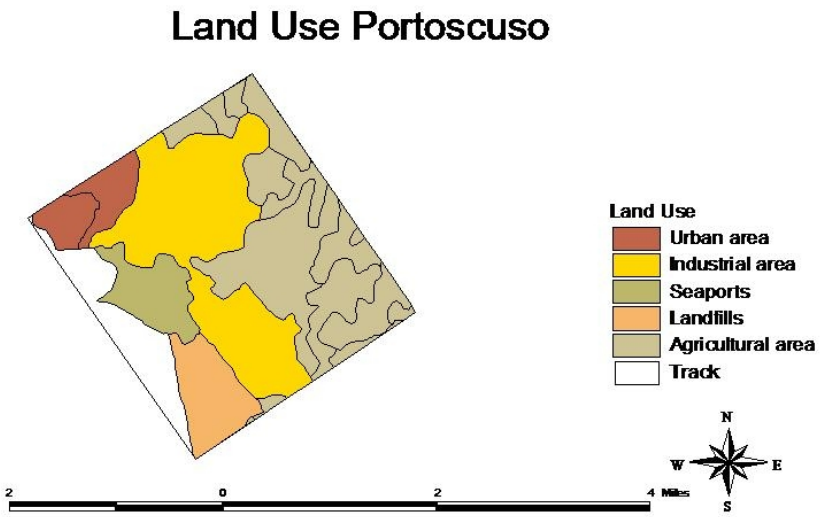

Figure 49: Soil use map over the flight domain: Portoscuso experiment.

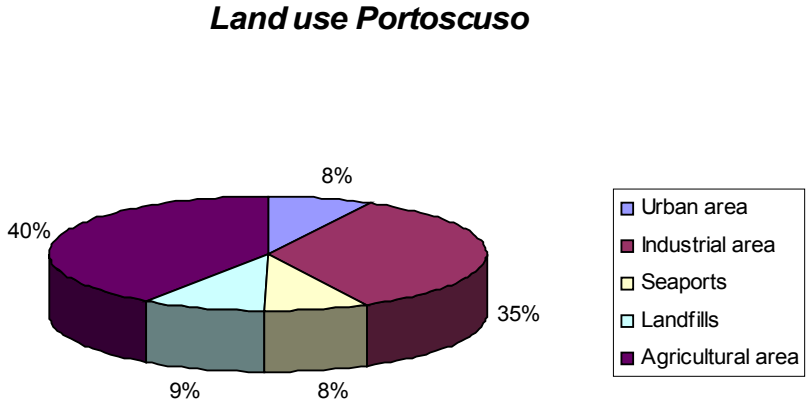

Figure 50: Percentage of macro-areas over Portoscuso flight domain

The assumption to neglect the entrainment transport holds since a strong inversion in CO_2 concentration profiles was detected with a greater content of the gas inside the mixed layer. This means that the contribution to the vertical turbulent transport is very small or null.

6.2.2 Machiareddu experiment: result and discussion

Industrial area of Machiareddu represents a small percentage of the total domain covered by aircraft (Figure 51). On the south-west corner of the domain is located the conservation area "Santa Gilla". It comprises a wetland that is also part of the flight domain. Machiareddu industrial pole is bordered by an agricultural area.

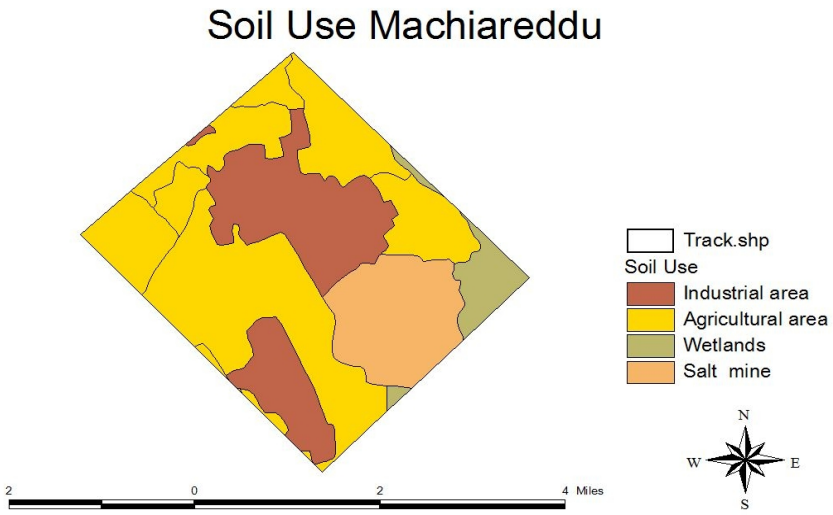

Figure 51: Soil use map over the flight domain: Machiareddu.

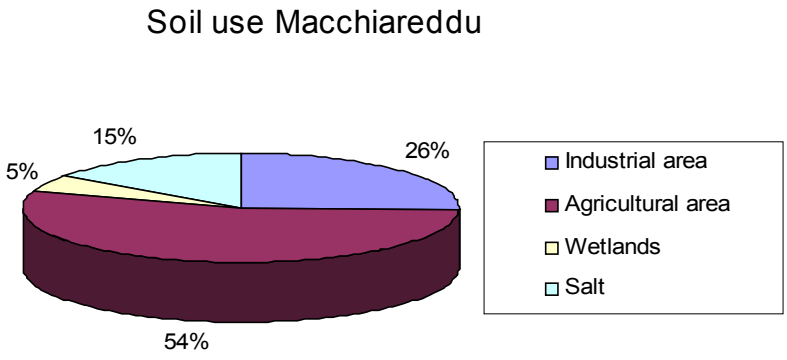

Figure 52: Fractions of land uses on the entire flight domain: Machiareddu.

In the following the results from mass balance approach are exposed relating to the area of Machiareddu. It was expected that the photosynthetic activity from cropland area could in part balance the emission produced by the industrial pole. The estimated CO_2 surface flux turn out to confirm the hypothesis.

In Table 7 are shown the results from Shepard method interpolation as function of top height of the virtual box and horizontal resolution.

Because of the high spatial heterogeneity of CO_2 concentration observed above the mixed layer height it was not possible to indicate an H_{top} height greater than 250 m. It was found that estimated fluxes are very variable as function of height, if H_{top} is greater than 280 m.

H_{top} (m)	***65***	***32.5***	***16.3***	***8.1***
210	9.88	10.22	10.69	10.42
220	9.94	10.40	10.83	10.48
230	10.00	10.58	10.98	10.54
240	10.06	10.76	11.12	10.60
250	10.13	10.94	11.26	10.66
260	10.19	11.12	11.40	10.72
270	10.25	11.30	11.54	10.78
280	10.31	11.48	11.68	10.84

Table 7: Estimated CO_2 surface fluxes in µmol/m2/s using Shepard interpolation as function of resolution and top height: area of Machiareddu.

In this case, estimated CO_2 surface fluxes came out from Bayesian method reveals a greater emission than that obtained by Shepard approach, though values are still in line with expectations. Median values obtained from MCMC iterates is equal to 14.93 µmol/m2/s (Figure 53).

It was detected a large inhomogeneity in wind and CO_2 concentration measurements, especially in the horizontal direction. This is also reflected in the variability in the results as function of height $\mathbf{H_{top}}$, in the layers above the inversion.

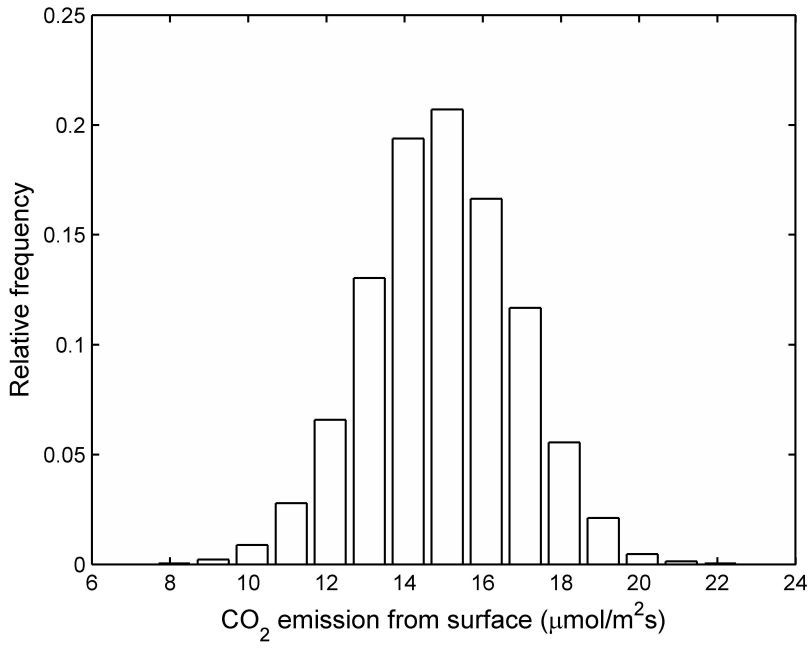

Figure 53: Relative frequency of CO_2 area averaged surface fluxes estimated as function of McMC iterates: area of Machiareddu.

Results from mass balance approach seem to be reasonable considering the surface characteristics of the flight domain.

Observing the CO_2 vertical profiles it could not be done a prevision about the strength of entrainment term in affecting the total balance. CO_2 concentration seems to be quite constant as function of height.

6.2.3 Cagliari experiment: result and discussion

Flight domain over the city of Cagliari comprises an urban area (about 50% of the total surface sampled) and a mixed agricultural area that occupy another 45%. The rest is a part of the Molentargius regional park, a wetland located on the south of the flight domain (Figure 40). In section 6.1.3 it was pointed out that the observed vertical CO_2 profile indicates a probable CO_2 sink. This is also confirmed by estimations given by mass balance. Though the area of Cagliari is the most urbanized of the region, the neighbouring surface seems to contribute to a net absorption of CO_2.

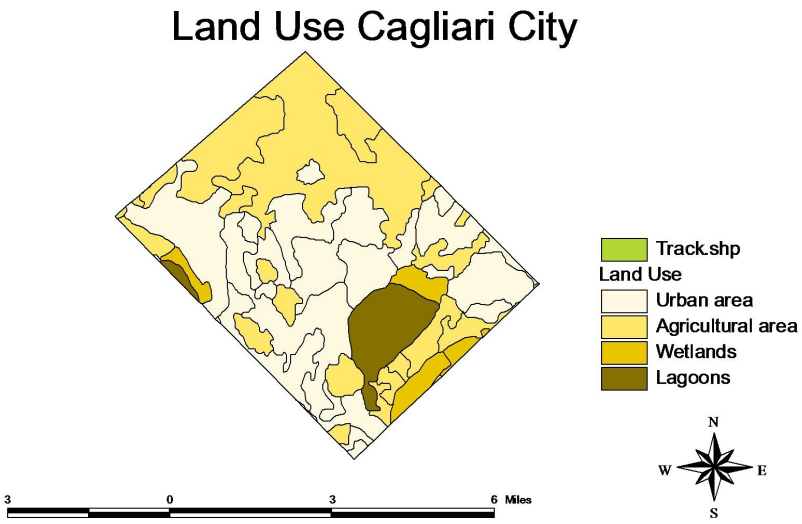

Figure 54: Land use map of the flight domain: Cagliari city.

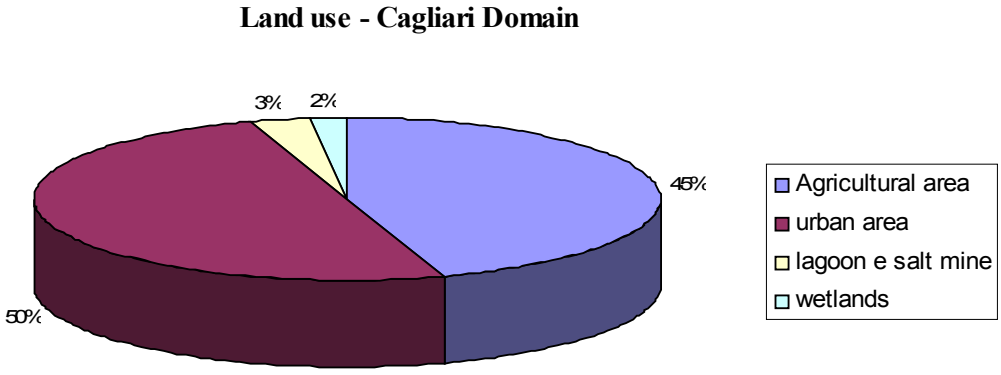

Figure 55: Fractions of land use over the flight domain: Cagliari city.

Both Bayesian and Shepard approach have given a negative balance. Median values resulted by McMC iterates was equal to -12.91 µmol/m2/s (Figure 55) with a very small range of variability as function of McMC iterates (interquartile range spanning $-17.17 \div -11.1$ µmol/m2/s.

In Figure 56 are showed Shepard method results as function of resolution of the interpolation grid and height H_{top}. .

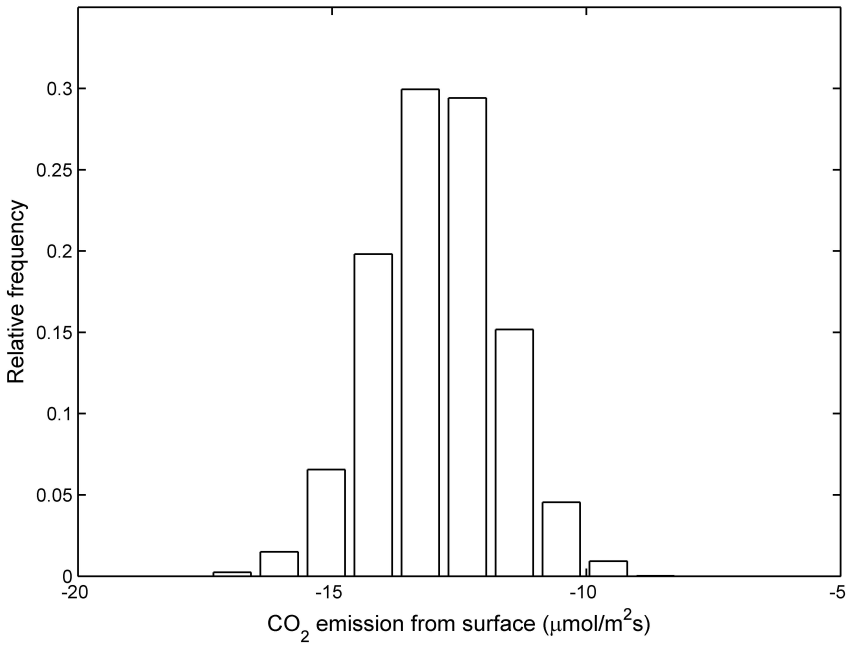

Figure 56: Hystogram of estimated CO_2 surface fluxes as function of Markov chain iterations: Cagliari city

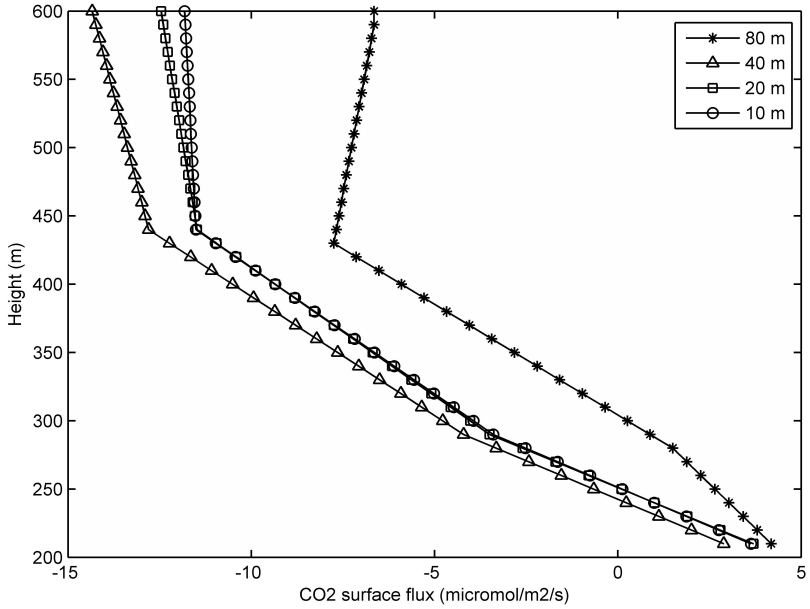

Figure 57: Estimated CO_2 surface fluxes plotted as function of the height H_{top}: Cagliari city.

As could be note the smaller horizontal resolution used is 80 m. These choose affects the results, given a not good representativeness of the wind and concentration fields over the integration volume. Increasing the horizontal resolution, the results from mass balance seem to converge to the same values (as was also observed in the other field cases). Above 450 m heights (altitude chose as top box closure) the estimated CO_2 surface fluxes seems to be constant with height. This confirms that if the sampled atmosphere in the higher layer is stable and there is any wind and concentration gradient in the horizontal direction the results are not affected by the choose of the top height.

Considering a horizontal resolution of 10 m CO_2 surface flux over the domain is estimated to be about – 12 μmol/m2/s.

In this case entrainment flux could play an important rule since the CO_2 concentration detected above the mixed layer height are greater than in the lower layers. The CO_2 vertical profile (Figure 41) is typical of a boundary layer where the surface act as a sink of the gas, while the top flux contribute to enrich of CO_2 the mixing layer.

Errors in CO_2 surface flux estimation

This work was focused on testing the mass balance methodology. The results show reliable results and in same case well agreement if compared with other methods or estimations. However there are still uncertainties about its validity. Errors associated to the estimation of CO_2 fluxes determined by mass balance mainly depend by assumptions required by model. In the following there will be discussed the latter and further sources of error:

Entrainment

In these applications the vertical turbulent flux on the box top is neglected assuming that top height of the virtual volume is located in the entrainment zone or in a stable layer, where turbulence is supposed to be absent. In same cases it's not possible to identify a defined inversion so as the turbulent flux term could have an important effect on total balance estimation. The estimation of entrainment flux is a difficult task because of the difficulty in sampling inside the entrainment zone where the turbulence is highly intermittent. However it's possible to use same parametrization

that, in any case, implies the use of atmospheric measurements or models in order to estimate some terms.

Measurements errors

Measurements errors could cause an important source of uncertainty in total balance estimation. This occurs especially if detected differences in CO_2 concentrations and wind values between the downwind and upwind side are small. The effect of the measurements errors on the total balance has to be mainly related to its propagation in applying calculation procedures (regression).

Bayesian McMC approach has the potentialities to take into account an uncertainty term due to the assumption done in the model and measurement errors. Instead, error propagation from the single measures to the final estimation of the surface fluxes should be done in the case of Shepard method.

Errors due to the assumptions of the model

An important source of error could be due to the steady state assumption made in the model. Aircraft does not fly the different box at the same time so as the atmospheric conditions could change considerably during the period of flight that usually has the duration of about one hour (or more). Problem should be resolved employing different flight strategies. More specifically it could be opportune to use two aircraft to perform the flight mission so as downwind and upwind sides of the area of interest could be monitored at the same time, limiting the problem related to steady state assumption.

A further limit in the application of the methodology should be also the not representativeness of the turbulent fields sampled over the leg flown by aircraft. Legs should be repeat several times to obtain a good representativeness of data over the entire domain. Obviously this is not possible if a single aircraft is used during a mission.

Chapter 7: Experiments in Forli city: "La Selva" area.

In the previous chapter has been described several case studies with the common characteristic to be located close to the coast. Complications occur in estimating surface fluxes by mass balance approach due, in same case, to the identification of the boundary layer (or CIBL) height. The latter question indirectly depends from the stratification occurring during sea breeze events.

In the following, calculation of are averaged CO_2 surface fluxes is done in different surfaces and atmospheric conditions.

The experiments examined in this chapter were conducted in two different period of time over an industrial area close to the city of Forli. The first mission, focused to the mass balance application and the second one to characterize the spatial gradient of CO_2 fluxes over the area using Eddy Correlation method. A tentative to estimate surface CO_2 fluxes was done by the application of LLF+ IM method.

7.1 The experiments

"La Selva" area is located in Northern Italy close to the city of Forli. The domain comprises an industrial centre in the north-west side, dominated by high anthropogenic activity and covering about 30% of the entire study area. Cropland dominates the remaining 70% (Figure 58).

Figure 58: Satellite image of "La Selva" area and representation of way points selected for mass balance mission.

Two flight experiments were carried out over the area under study. The first one, performed in the summer 2005, was devoted to the application of mass balance approach. In this case the aircraft flown over the area described a square shape pattern at five different altitudes on the base of the typical "mass balance trajectory", explained in section 4.3.1. This case study will be named in the following "case study 1". Second flight mission was performed during a spring day (May 2006) and was addressed to the calculation of Eddy covariance fluxes ("case study 2") over the area. This flight experiment was devoted to the identification of the CO_2 flux patterns over the area and the identification of the single contributions from different land use typologies.

7.1.1 Case study 1

The flight campaign was performed on 16 September 2005 with take off at 12:58 UTC. Five rectangular patterns at 125, 337, 527, 741 and 965 meters were flown by the aircraft, bordering the selected area. Two profiles were performed upwind and downwind the boundaries (Figure 59). Boundary Layer height was estimated on the base of profiles observation and applying the considerations discussed in 2.2.2.

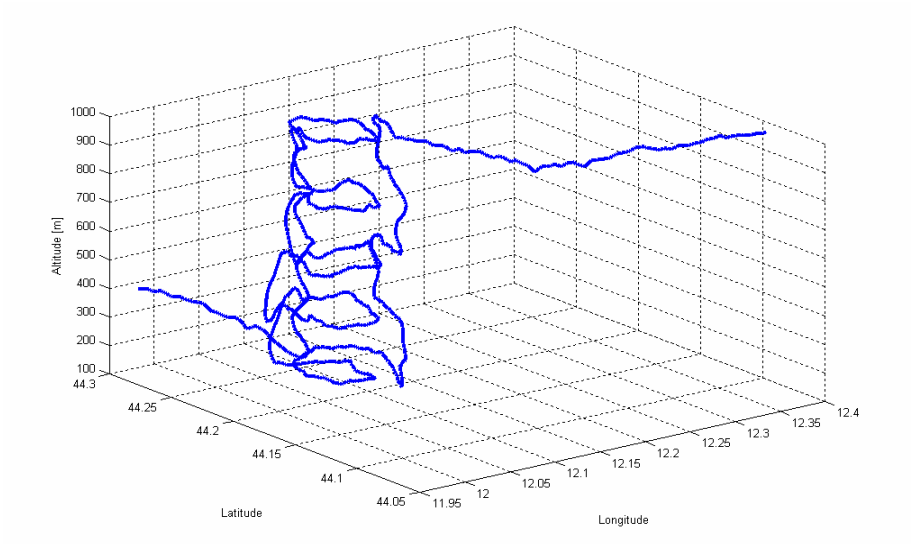

Figure 59: Flight trajectories flown on 16 September 2004 over "La Selva".

For any given profile can be difficult identifying inversions due sometimes to the low SNR of the signal, especially in situation involving weak surface heating or complex synoptic flow, as in the case under study. Cloudy condition occurs for the entire period of flight, evident from temperature and humidity stratifications, especially in the upwind sounding (see Figure 60).

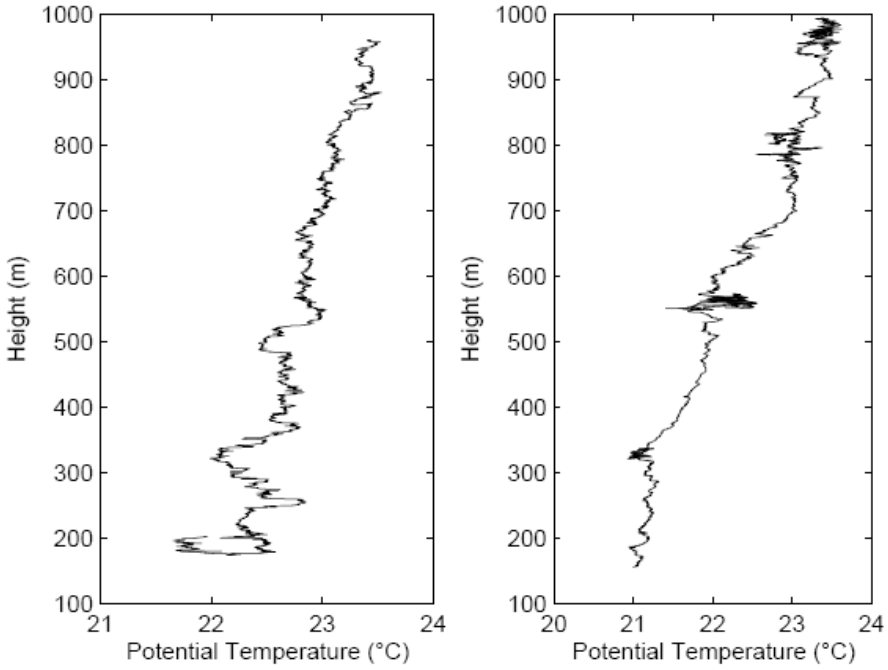

Figure 60: Potential temperature vertical profiles data sampled over "La Selva" on 16 September 2005.

Two inversions occur at about 300 and 500 m and the identification of the marked temperature inversion, typical of convective situation, become difficult. A more defined increase in potential temperature is evident in the downwind profile flown at the end of campaign. Presence of clouds dominates the first period of the sampling as shown by Net radiation time series, acquired during the campaign, where an increment in solar radiation is observed (Figure 61). Profile flown at the end of the campaign shows a more evident enhancing of potential temperature at about 500 m height.

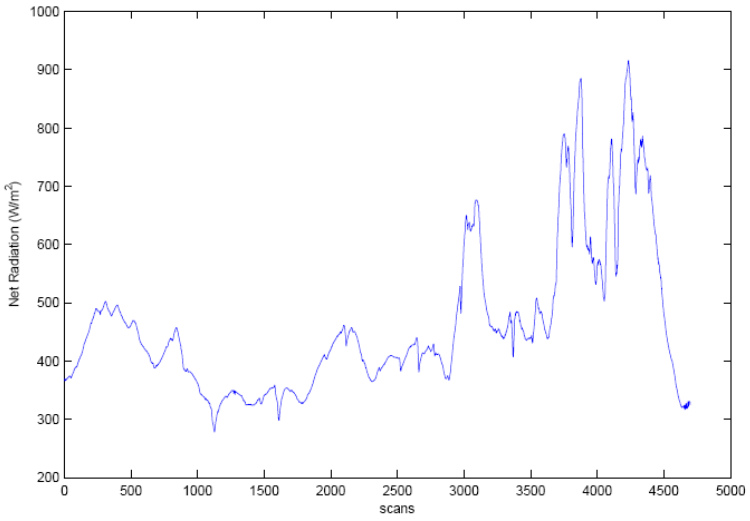

Figure 61: Net radiation (W/m2) measured during the whole flight.

7.1.1.1 Mass balance application: results and discussions

In Table 8 results from Shepard method application are shown. As in the previous applications (Chapter 5:), the results are analysed as function of estimated top height of the virtual box and horizontal resolution of the interpolation grid.

The altitudes chosen as virtual box top are comprised between 450 and 550 m. Results are quite stable as function of altitude. Instead, the variability of the results as

function of horizontal resolution seems to be more randomly distributed that respect to the previous applications (mainly due to the greater vertical distance between the boxes flown by the aircraft).

top height	*horizontal resolution (m)*			
(m)	45	22.5	11.3	5.6
450	13.71	13.79	12.86	13.41
470	13.58	13.75	12.60	13.17
490	13.44	13.72	12.34	12.93
510	13.31	13.68	12.07	12.70
530	13.18	13.64	11.81	12.46
550	13.05	13.60	11.55	12.23

Table 8: CO_2 averaged surface fluxes (µmol/m2/s) estimation resulted from the application of Shepard method. Results are showed as function of top height and horizontal resolution of the interpolation grid

On the left panel of Figure 62 horizontal mean fluxes interpolated by Bayesian method (black line) are plotted against measured data, while on the right panel are represented, as histogram, the CO_2 average surface fluxes estimated from MCMC iterations. The median value is 11.5 µmol/m^2/s with an interquartile range spanning the interval $11.2 \div 11.8$ µmol/m^2/s.

CO_2 fluxes estimated by the two interpolation methods are comparable. The results obtaining using Shepard function has a tendency to be greater of about 1-2 µmol/m^2/s than that achieved by Bayesian approach interpolation.

The estimation of CO_2 area averaged surface flux is realistic if we consider that the great part of the area is composed by croplands that contribute to absorb part of the CO_2 emission from the industrial areas. Note that we could expect a great photosynthetic activity from vegetated surface, being the campaign performed in summer time. A detailed description of the contributions from the different patches over the domain will be given from the results in case study 2.

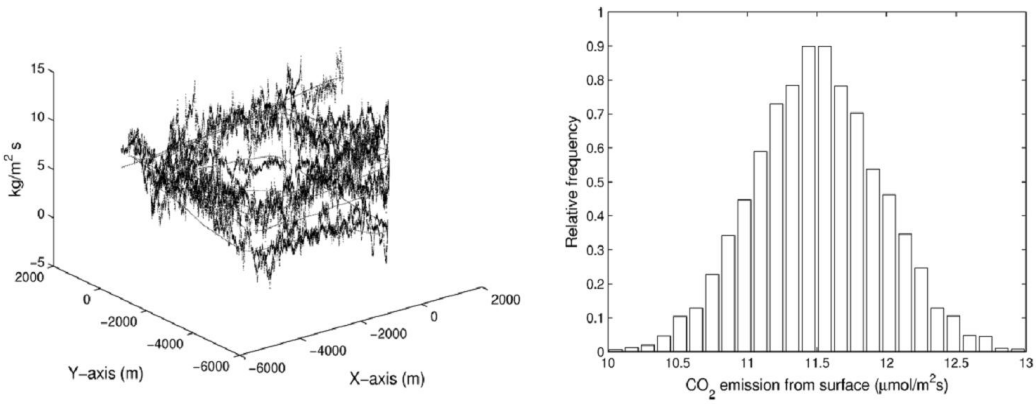

Figure 62: On the left side: horizontal flux interpolated by Bayesian approach (thin line represents the interpolated values). On the left: relative frequency of CO_2 fluxes estimates from MCMC iterates.

It was discussed about the possible clouds development extending above the BL. Updraft and downdraft associated with this phenomenon may have led to enhanced transport by entrainment thought the top of boundary layer. This was confirmed by a slight enhance of CO_2 along vertical profile. CO_2 jump was about 2 ppm. Assuming an indicative value of the entrainment velocity to be $\approx$ 1 to 3 cm, a rough estimation of the entrainment flux is between $0.8 - 2.5$ μmol/m2s.

7.1.2 Case study 2

Second mission was carried out on the 3rd of May 2006 and focused to the quantification of CO_2 emissions from industrial suburban area and photosynthetic absorption from the agricultural area that surrounds the industrial poles. In this manner it's possible to build up a source/sink inventory representative of the whole territory.

During the mission, started at 12:51 UTC, a grid shaped flight was performed over of the area under study. Track was flown at two different altitude, respectively 80 and 140 m AGL.

Figure 63 shows the grid performed by aircraft and the indication of the tracks (the numbers indicate the temporal succession of the legs).

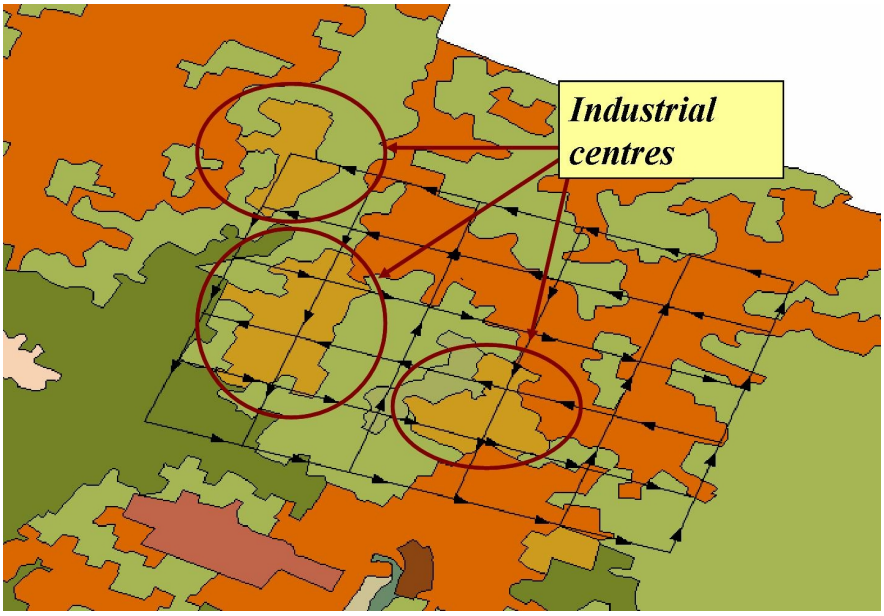

Figure 63: Soil use map over "La Selva" and indication of the main industrial centres (red circles).

Mission was planned so as to isolate the contributions of industrial centres from agricultural areas and the Forli downtown. Distance between each leg of the grid is about 1.5 km resulting in a total number of six straight and level patterns for each side of the flight domain. The length of the tracks was about 8 km in the direction East-West and 6 km in the direction North- South.

7.1.2.1 CO_2 surface fluxes calculated over "La Selva": results and discussion.

CO_2 surface fluxes have been calculated by Airborne Eddy Covariance Method. Each value has been extracted calculating eddy correlation over a window of 3 km, with an overlap of 1 km between each window.

A Steady state test is used to detect non steady state conditions, which is an assumption of Eddy Covariance method. This test compare 1 minute and half covariance (about 3 km) with the arithmetic means of the six 14 minute covariance in this interval. The agreement between both values is a measure of steady state condition. In this work are showed fluxes that have passed the "steady state test".

In Figure 63 are plotted interpolated values of CO_2 fluxes measured over the area. As can be note it is evident that emission coming from the industrial centres contributes to the total CO_2 surface flux with an emission of about 30 µmol/m2/s.
CO_2 sinks from agricultural area are variable between -1 and -10 µmol/m2/s but they covers a greater surface of the domain.

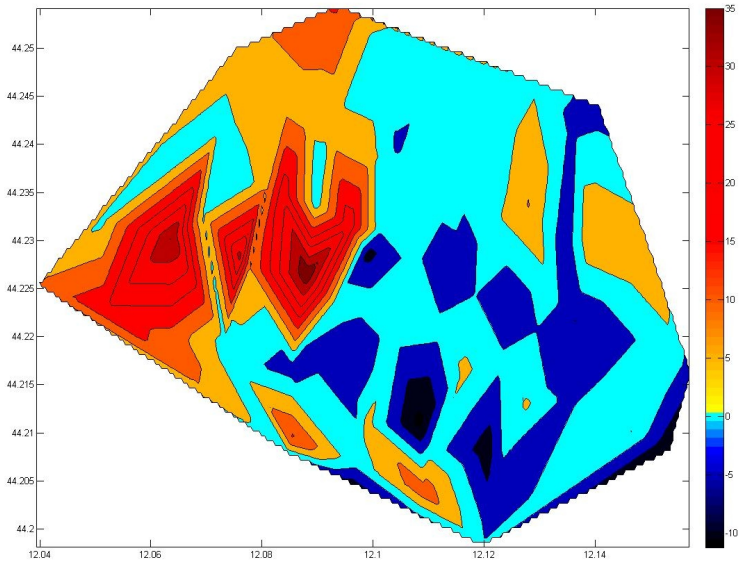

Figure 64: CO_2 fluxes calculated by Airborne Eddy Covariance over the lowest flight pattern interpolated over the entire flight domain.

7.1.2.2 Low Level Flight + Inverse Model Application: Result and discussion

The present study is devoted to the issue of determining area-averaged surface flux from a single low level flight. The method was applied by Bunge et al (2006) for the determination of area-averaged latent and sensible heat fluxes. In this study the approach is used for CO_2. Case study #2 was selected because a grid shaped pattern was performed. This allows to obtain more information about spatial gradients of the gas, a condition for which inverse modelling can work well.

For testing of the LFF+IM both flight levels sampled during the mission were used, having their flight altitude very close each other: the lowest was flown at 80 meters and the higher at 140 m. In Figure 65 flight tracks selected for applying the method are shown. Due to the worse performance of the airborne measurement system during manoeuvres, round patterns were cut off from data series.

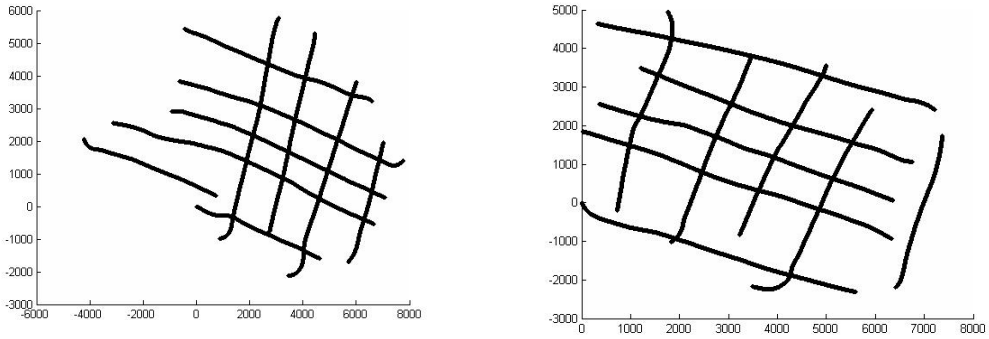

Figure 65: On the right: flight track selected from the grid flown at 80 m height. On the left: flight track selected from the grid flown at 140 m height.

Inverse model requires assumption about deviations of the parameters (4.8) and accuracy of the measurements. Moreover an a priori hypothesis about values of the parameters has to be given.

In this case study a priori parameters m_{prior} are given equal to:

$m_{0=}$ mean values of CO_2 concentrations; $m_{1=}0$; $m2_{=}0$; $m_{3=}0$; $m_{4=}0$;

Then, this means that CO_2 concentration is assumed to be constant in time and space. These a priori assumptions have a negligible effect on results because of the large number of measurements, so that the posterior is dominated by the likelihood.

As in empirical Bayes methods, standard deviation of parameters was calculated from a preliminary inspection of measured data.

Table 9 show numerical results for inverse modelling given for the parameters (4.8) for each flight grid.

Grid height (m)	m_0 (ppm)	m_1 (ppm/s)	m_2 (ppm/m)	m_3 (ppm/m)	m_4 (ppm/m)
80	367.03±0.447e-03	0.0002±1.618e-08	0.0001±0.445e-08	0.0003±0.554e-09	-0.0173±4.224e-06
140	369.10±1.161e-03	0.0003±4.346e-08	0.0001±0.344e-08	0.0002±0.224e-08	-.0188±7.2522e-06

Table 9: Estimated parameters m for the two low level flights. Numbers in parenthesis represent the standard deviations of model parameters, as identified by the model

.

In Figures 66 and 67 are shown the modelled **CO_2** fluxes starting from parameters

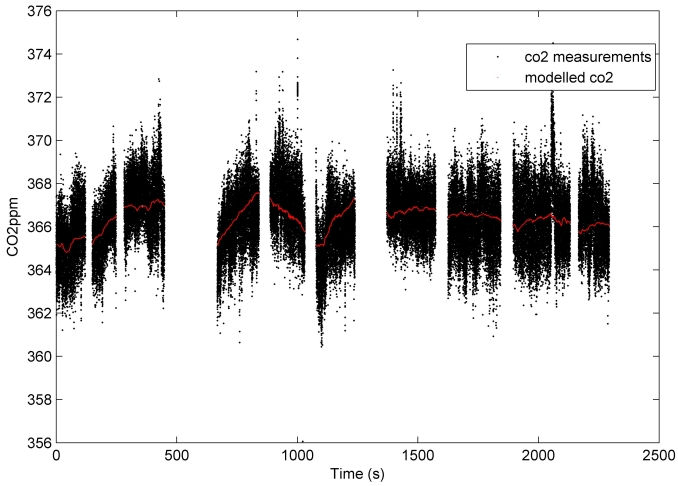

Figure 66: Time series of CO_2 concentration for the lowest flight level (80 m). Red line represents modelled CO_2 data.

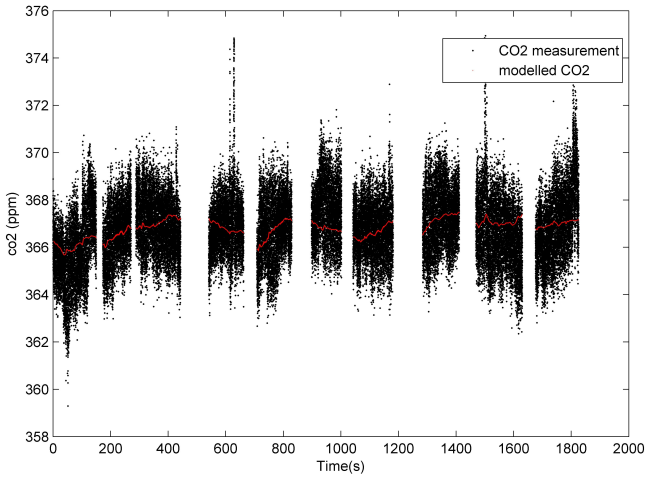

Figure 67: Time series of CO_2 concentration for the highest flight level (140 m). Red line represents modelled CO_2 data.

Once model parameters have been estimated, CO_2 surface flux is given by:

$$F_0 = \frac{\sum_{1}^{n}(w'CO_2') + (m_1 + m_2U + m_3V + m_4W)}{n}$$

Area average CO_2 flux extrapolated for the lower box (80 m) is equal to 11.87 µmol/ m2/s. On the higher level of flight (140 m) the estimated CO_2 surface flux is 10,30 µmol/m2/s.

Conclusions

The thesis work focused on the application of a methodology for trace gases fluxes estimation at territorial scale by using airborne data. The method has been developed for CO_2 fluxes estimation looking forward to apply it for different gases like N_2O and CH_4 over the Piana del Sele location. The carbon dioxide has been suitable for the testing purpose because of the high frequency features of the state of the art instrumentation available on the market, and already present on the airborne platform used for the different test campaigns already performed.

The methodology has been investigated since the Piana del Sele site is a coastal zone strongly influenced by the sea breeze. This phenomena is not well handled by other methodologies (i.e Convective Boundary Layer Budget as performed by Cleugh et al 2004, Laubach at al 2002, Schmitgen et al 2004) since most of those are considering the advection as a negligible term of the balance equation. In the case of the test sites investigated in this work, instead, the advection term is not negligible due to the presence of the sea breeze phenomena. In fact the behaviour of the coastal atmospheric environment is strongly influenced by it. In the "mass budget" technique both the gas concentration and wind direction and magnitude are directly measured at the boundary of the ideal box flown by the aircraft. This allows to implicitly treat the advection in the mass balance equation, and the advection became the most important term in finding out the final balance. Moreover the air inlet coming from the sea is poor in CO_2, and this feature allows to find great concentration difference between the up and downwind fields. That higher difference in concentration allows to minimize the potential errors due to the measurement technique itself (i.e. airborne sensors with less accuracy compared to those used for ground application).

Another important feature of the method compared with the CBLB is that it can be used without waiting for a well mixed boundary layer.

On the other hand, this method has to be applied only if the steady state conditions are satisfied. To cover the whole ideal box needed to estimate the surface emission with the mass balance method with small (and slow) aircrafts, as the one used in the work is, different hours are often needed. This could results in not satisfying the above mentioned "steady state" constraint.

As well known, to obtain the different terms of the "mass budget" equation, data continuity is needed over all the faces of the ideal box flown by the aircraft, over where the equation's terms are integrated. Due to the limited endurance of the aircraft as well as the steady state constraint, the aircraft flies 4-5 flight levels, sampling at the maximum frequency of 50 Hz. This sampling modality results in a very high sampling density along the single flight track level, but at the same time in a very poor density in the vertical direction. To overcome to this drawback regression techniques are needed. In this work two different methods have been investigated and applied to all the cases, evaluating the impact applying different regression philosophies. In fact the first regression technique is from a deterministic family, while the second is from a stochastic one. In the most part of the case analysed, the results applying the different technique did not show big difference. The two techniques did not agree when very strong and narrow gas plumes are present in the monitored area (i.e. chimney). In this case the deterministic technique seems to be less affected from the presence of the plume, while the stochastic one shows the opposite behaviour. This could lies with the not correct estimation of the parameters of the similarity lows (Ratto et al, 1994) used in Bayesian inversion.

In this work the method has been applied to four coastal test sites plus an inland one. The possibility to apply the method to an enough number, in terms of statistical meaning, of test sites gave the opportunity to better evaluate the potentialities of the method and at the same time its limits. In all the investigated sites the method results are all reasonable, when analysed in terms of land-use percentage and when possible compared with other measurements techniques like the well established eddy covariance. For some cases comparing the results with annual "database emissions inventory" also resulted in a reasonable agreement.

Even if in this work enough number of case studies were analyzed, and the goodness of the method has been proved, the method has still to be better evaluated. A better assessment of the different terms has to be done as a next step. Even thought that from the first preliminary evaluation shown in this work, seems that the entrainment term don't have an important impact on the balance, especially when the top of the ideal box is selected to be above the boundary layer top (Wratt et al, 2000), it remains one of the most difficult terms to treat. The main difficulty is due to the fact

that is not easy to foresee where the height of the BL will be during the mission, and therefore where the aircraft has to fly to acquire data in that very thin zone. The best approach, under evaluation for the incoming missions, is the use of a ground based lidar for the real time measurement of the boundary layer top, in this way would be easy to measure the entrainment vertical velocity by using the airborne platform and therefore evaluate the weight of this term in the whole balance equation.

The next step of the work is to find out the accuracy of the method, starting from the analysis of the error propagation from the single measures to the final estimation of the surface fluxes, particularly referring to the Shepard method. Another important point is the validation of the method using another independent measurement that can be considered as reference. The strategy to adopt could be the one used in the "Forli" case study already presented in this work, where the comparison between the airborne eddy covariance and the mass balance methods have been showed. The step further should be performing both the measurements simultaneously, ideally by using two airborne platforms at the same time.

References

Amato,U., M.F. Carfora, S.M. Alfieri, M. Esposito, V. Magliulo, 2007. Metodologia di bilancio di massa per la stima degli scambi gassosi superficiali a scala territoriale. Volume *Clima e cambiamenti climatici: le attività di ricerca del CNR.*

Ahlonso E.,, Ding Y. , Schimel D (2001). The Climate System: an Overwiev. In : Climate Change. The Scientific basis. Contribution of Working Group I to the Third Assessment Report of the IPCC.

Arya, S.P, 2005. Micrometereology and Atmospheric Boundary Layer. Pure appl. Geophys. Birkha¨user Verlag, 162:1721-1745.

Bange J., Zittel P., Spieß T., Uhlenbrock J., and Beyrich F.,: 2006, A NewMethod for the Determination of Area-Averaged Turbulent Surface Fluxes from Low-Level Flights Using Inverse Models. Boundary-Layer Meteorol., DOI: 10.1007/s10,546–005–9040–6.

Bange J., Herold M., Spieß T., Beyrich F., and Hennemuth B., 2006**:** Turbulent Fluxes from Helipod Flights above the Heterogeneous LITFASS Area. *Boundary-Layer Meteorol.*, 121: 127-151.

Cleugh, H.A., M.R. Raupach, P.R. Briggs and P.A. Coppin (2004). Regional-scale heat and water vapour fluxes in an agricultural landscape: an evaluation of CBL budget methods in OASIS. *Boundary-Layer Meteorol., 110,* 99-137.

Crawford, T.L. and R.J. DOBOSY (1992): A sensitive fast response probe to measure turbulence and heat flux from any airplane, Boundary-Layer Meteorol., 59, 257-278.

Crawford, T.L., Dobosy, R.J., McMillen, R.T., Vogel, C.A., Hicks,B.B. (1996). Air-surface exchange measurement in heterogeneous regions: extending tower observations with spatial structure observed from small aircraft. Global Change Biol. 2, 275-285.

Deardorff, J. W. (1980), Stratocumulus-capped mixed layers derived from a three dimensional Model, Bound. Layer Meteor., 18: 495, 527.

Gelfand, A.E., Zhu, L., Carlin, B.P., 2001. On the change of support problem for spatio-temporal ata. Biostatistics 2, 31–45.

Gilks, W.R., Richardson, S., Spiegelhalter, D.J., 1996. Markov Chain Monte
Carlo in Practice. Chapman and Hall/CRC, Boca Raton, Florida.

Gioli B, Miglietta F (2007). Stima del bilancio del carbonio a scala regionale. Forest@ 4 (4): 469-477. [online] URL: http://www.sisef.it/forest@/

Grunwald, J., N. Kaltho_, U. Corsmeier, and F. Fiedler: 1996, `Comparison of Areally Averaged Turbulent Fluxes over Non-Homogeneous Terrain: Results from the EFEDA-Field Experiment'. Boundary-Layer Meteorol. 77, 105-134.

Gryning, S. E., and E. Batchvarova, Analytical model for the growth of the coastal internal boundary layer during onshore flow, Q.J.R. Meteorol. Soc., 116, 187-203,1990.

Heffter, J. L. (1980), Transport Layer Depth Calculations, Second Joint Conference on Applications of Air Pollution Meteorology, New Orleans, LA.

Horst TW, Weil JC (1992) Footprint estimation for scalar flux measurements in the atmospheric surface layer. Boundary-Layer Meteorology, 59, 279–296.

Kalthoff, N. ,Corsmeiera, U., Schmidta, K. , Kottmeiera, Ch., Fiedlera, F., Habramb,M., Slemrb, F.:2002 “Emissions of the city of Augsburg determined using the mass balance method”. Atmosph. Environment. 36, S19-S31.

Kienele, M. , Atchinson K., and Masters, S. (1985), Worldwide Climatological Maximum Mixed Layer Heights, DCS-ATR-84-74, ENSCO, INC.

Laubach, J., Fritsch, H. (2002), Convective boundary layer budgets derived from aircraft data. Agricultural and Forest Meteorology. 111, 237-263.

Lilly D. K (1968), Models of cloud-topped mixed layers under a strong inversion. Quart. J.Roy. Meteor., 94, 874-884.

Melas,D. , and H.D. Kambezidis, The dept of the internal boundary layer over an urban area under sea-breeze conditions, Boundary Layer Meteorology, 61,247-264,1992.

Miller, S. T. K., B. D. Talbot, and H. Mao (2003), Sea Breeze: Structure, forecasting, and impacts, r*eviews of Geophysics*, Vol. 41, No. 3, doi:10.1029/2003RG000124.

Oke, T.R. (1987), Boundary Layer Climate. Second Edition, New York, Routledge.

Ratto , C.F,, Festa, S., Romeo, C., Frumento, O.A, Galluzzi, M. (1994): Mass consistent models for wind fields over complex terrain: the state of art. Environmental Software 9,247-268.

Riccio,A, G. Giunta, S.M. Alfieri, M. Esposito, V. Magliulo, 2007. Un approccio Bayesiano per la stima del flusso superficiale di CO_2 a partire da misure rilevate da piattaforma aerea. Volume Clima e cambiamenti climatici: le attività di ricerca del CNR.

R.L. Petersen, (1999): Development and evaluation of an improved algorithm for estimating Thermal Internal Boundary Layer Height. Cermak Peterka Petersen, Inc., 1999

Schmitgen, S., H. Geiss, Ph. Ciais, B. Neininger, Y. Brunet, M. Reichstein, D. Kley and A. Volz-Thomas (2004). Carbon dioxide uptake of a forested region in southwest France derived from airborne CO_2 and CO measurements in a quasi-Lagrangian experiment. *J. Geophys. Res., 109,* D1403, doi : 10.1029/2003JD004335.

Seibert P., Beyrich F., Gryning S.E., Joffre S., Rasmussen A. and Tercier P. (2000), Review and intercomparison of operational methods for the determination of the mixing height, Atmospheric Environment, 30, 1001-1027.

Shepard, D. (1968), A two dimensional interpolation function for irregularly-spaced data. ACM National Conference, 517-524.

Stull, RB, 1988. An Introduction to Boundary Layer Meteorology. Kluwer Acad. Publ. Dordrecht, 666 pp.

Sugiyama G., Nasstrom J. (1999), Methods for Determining the Height of the Atmospheric Boundary Layer, Lawrence Livermore National Laboratory Internal Report UCRL-ID-133200.

Sullivan, P., Moeng, C., Steven, B., Lenshow, D.H., Mayor, S.D. (1998), Structure of the Entrainment Zone Capping the Convective Atmospheric Boundary Layer, Journal of the Atmospheric Science, 55: 3042, 3063.

Talbot C., P. Augustin, C. Leroy, V. Willart, H. Delbarre and G. Khomenko, 2007: “Impact of a sea breeze on the boundary-layer dynamics and atmospheric stratification in a coastal area of the North Sea”, Boundary-Layer Meteorology, DOI : 10.1007/s10546-007-9185-6, 133-134.

Webb, E., G. Pearman, and R. Leuning. 1980. Correction of flux measurements for density effects due to heat and water vapour transfer. Q. J. R. Meteorol. Soc. 106:85–100.

Weisman, Response to: On the Criteria for the Occurrence of Fumigation Inland from a Large Lake. Atmospheric Environment, 12, (1976) 172–173.

Wratt, D.S., Gimson, N.R., Braisford, G.W., Lassey,K. R., Bromley A.M, Bell, M.J. (2000), Estimating regional methane emissions from agriculture using aircraft measurements of concentration profiles. Atmosph. Environment. 35, 497-508

Taylor, G. I. 1921. Diffusion by Continuous Movements. *Proc*. *London Math*. *Soc.* **20**: 196.

Tennekes H. (1973), A model for the dynamic of the inversion above a convective boundary. J. Atmosf. Sci., 30, 558-567.

Acknowledgements

I would like to thank my tutor Angelo Fierro for his advice, guidance and encouragement.

Special thanks to Francesca Carfora and Umberto Amato for their help and for the time spent in performing Shepard method.

Thanks to my tutor Prof. Angelo Riccio for the work dedicated to the implementation of Bayesian Markov Chain Montecarlo method.

I also would like to thank my tutor Vincenzo Magliulo for giving me the possibility to achieve this research.

Many thanks to Prof. Menenti for the support.

I would like to express my gratitude to Teresa Bertolini and Paul Di Tommasi for providing meteorological data of "Borgo Cioffi" site.

Thanks to Stephan De Roode for his patience and very useful lessons about boundary layer meteorology.

Thanks to my colleagues Paolo Donnarumma for the technical support in performing aircraft measurements and Maurizio Buonanno for his precious advices.

Thanks to the pilot Paolo Troisi for performing the mission over Piana del Sele and Franco Romagnoli for its great performance during the missions in Sardinia.

Thanks to all the people that in same way have given a contribute to achieve this work… and also thanks to an unknown reviewer for his very useful suggestions.

Thanks to my colleagues: Michele, Silvia, Lucia and Luca for the breaks and the funny chats.

Thanks to my family for their moral and economic support and to my wonderful nephew Silvia.

Finally, I want to thanks a special person: Marco, for being my guide and my fellow during these tree years and for the beautiful days spent together around Europe.

His encouragements gave me the strength to write this thesis and to overcame a so difficult period of my life. This thesis is dedicated to him.